

The Possible Alleviating Effect of Granulocyte-Colony Stimulating Factor (G-CSF) on High Fat Diet-Induced Cardiomyopathy in Albino Rat: Histological, Immunohistochemical and Ultrastructural Study

Original
Article

Sara Magdy Abd Elhady Elsaeed, Shehab Hafez Mohamed, Nesreen Moustafa Omar and Eman Shaaban Abdel-Aziz Abul-Ela

Department of Medical Histology and Cell Biology, Faculty of Medicine, Mansoura University, Mansoura, Egypt

ABSTRACT

Introduction: Prolonged intake of a high-fat diet (HFD) is typically linked to obesity and increased risk for multiple pathologies including type II diabetes mellitus, cardiovascular disorders, hypertension, and hyperlipidemia. Granulocyte-colony stimulating factor (G-CSF) is a polypeptide cytokine involved in the basic control of neutrophils production.

Aim of the Work: The current study was performed to investigate the role of G-CSF on HFD-induced cardiomyopathy in a rat model.

Materials and Methods: Thirty adult male albino rats (200-220 gm) assigned into 3 groups were used. Group I (Control group): fed on a standard diet for 14 weeks. Group II (HFD group): fed on HFD for 14 weeks. Group III (HFD + G-CSF) fed on HFD for 14 weeks and given G-CSF (200 µg/kg/day) intraperitoneally once daily for 5 successive days starting after 12 weeks of HFD intake. Specimens from the left ventricle and right atrium were obtained and processed for light and electron microscopic studies. Biochemical, histomorphometric and statistical studies were performed.

Results: HFD group showed marked degenerative changes in the cardiac muscle both at the light and electron microscopic levels. These changes were accompanied by significant increases in tissue MDA level and area percentage of collagen and caspase-3 immune expression. On the other hand, HFD + G-CSF group displayed improvement in the cardiac muscle histology together with reductions in tissue MDA level and area percentage of collagen and caspase-3 immune expression. Upregulation of CD117 immune expression was also observed in this group.

Conclusion: G-CSF could significantly mitigate HFD-mediated cardiotoxicity via antioxidant, anti-apoptotic, anti-fibrotic impacts and recruitment of stem cells derived from bone marrow to injured tissues.

Received: 23 January 2024, **Accepted:** 23 March 2024

Key Words: Cardiomyopathy; caspase-3; C-kit, G-CSF; HFD.

Corresponding Author: Sara Magdy Abd Elhady Elsaeed, MSc, Department of Medical Histology and Cell Biology, Faculty of Medicine, Mansoura University, Mansoura, Egypt, **Tel.:** +20 10 6498 8711, **E-mail:** saramagdy@mans.edu.eg

ISSN: 1110-0559, Vol. 48, No. 1

INTRODUCTION

People's food and lifestyle habits have been changed significantly as modern civilization developed, leading to a rise in the consumption of junk food with high fat content in both urban and rural regions.^[1] Chronic consumption of a fat-rich diet is typically linked to obesity, which is regarded as a substantial risk factor for many pathologies including type II diabetes mellitus, cardiovascular diseases, hypertension, and hyperlipidemia. The abnormal lipid accumulation in the pancreas, liver, kidney, heart, and other non-adipose organs arises from an imbalance between the amount of energy consumed and the amount of nutrients ingested.^[2,3] High fat diet causes significant pathological conditions including inflammation, oxidative stress, lipid metabolic disorder, apoptosis, and hyperlipidemia contributing to higher prevalence of cardiovascular disorder.^[4,5]

Granulocyte-colony stimulating factor (G-CSF) is a polypeptide cytokine implicated in the basic control of neutrophils production. Hematopoietic cells have been shown to be stimulated by G-CSF to survive, divide, and differentiate.^[6] Clinically, G-CSF is utilized to release hematopoietic stem cells (HSC) into the peripheral blood making it essential for autologous transplantation of peripheral blood stem cells.^[7] Previous workers showed that G-CSF can improve the cardiac function by attracting stem cells from bone marrow, encouraging angiogenesis, decreasing apoptosis, and adjusting the amount of collagen in injured hearts.^[8]

Most of the previous G-CSF studies have been conducted on various ischemic cardiomyopathy models. Regarding non-ischemic cardiomyopathies, little is known concerning G-CSF's possible cardio-protective effects. Thus, the purpose of this research was to examine the

histological, immunohistochemical, and ultrastructural alterations in the cardiac muscle of adult male rat fed on fat rich diet and to assess the role of G-CSF in the mitigation of these alterations as well as its role in the promotion of repair mechanisms.

MATERIALS AND METHODS

Chemicals

A. Drugs

Recombinant human G-CSF (Filgrastim) (trade name: Neupogen prefilled syringe): was obtained from the Egyptian Sigma Company. It is accessible in the form of (30 MU /0.5 ml; equal to 300 micrograms/0.5 ml) prefilled syringe and administered at a dosage of 200 µg/kg/day by intraperitoneal injection once daily for 5 successive days by the completion of the 12th week.^[9]

B. Kits

- Anti-caspase 3 antibody was a class IgG rabbit polyclonal antibody (catalog number: GB11532, Servicebio, Olympia Avenue, Woburn, USA).
- Anti-CD117 (C-kit) antibody was a class IgG rabbit polyclonal antibody (catalog number: 60-0020-7, Sakura Finetek, USA).

Experimental Animals

Thirty adult male albino rats, three months old, weighing between 200 and 220 grams were acquired from the animal house present in Faculty of Pharmacy, Mansoura University. The rats were kept in metal cages with smooth wood fragments in a carefully monitored laboratory environment with a 12-hour light/dark cycle and a temperature of 25°C. Every animal received a standard pellet diet. Water was available to all animals without restriction. Three rats will be kept apart in their own cages to avoid crowding.

Location of the research project

The present research study was done at Department of Medical Histology and Cell Biology, Faculty of Medicine, Mansoura University. It was executed in compliance with the worldwide guidelines for usage and preservation of experimental animals. It was granted acceptance by the Institutional Research Board (IRB) of Faculty of Medicine, Mansoura University (MS.21.03.1408).

Animal groups

Three equal groups were randomly selected as follows:

Group I (control group) (n = 10): The rats in this group were fed on a standard diet (66% carbohydrates, 17 % proteins, and 17 % lipids) for 14 weeks.^[10]

Group II (HFD group) (n =10): The rats in this group were fed on a high-fat diet (HFD); 43% carbohydrates, 14% proteins, and 43% lipids [10] for 14 weeks.

Group III (HFD + G-CSF group) (n =10): The rats

in this group were fed on the same HFD as group II for 12 weeks. Thereafter, 200 µg/kg/day of G-CSF was given by intraperitoneal injection once daily for 5 consecutive days^[9]. After that, the rats continued feeding HFD up to the end of the 14th week.

Procedure for tissue processing and obtaining samples

At the completion of the experiment (at the end of the 14th week), rats from every group were given ether inhalation anesthesia. A dissection of the heart was done. The ventricles were divided into rings, 1–2 mm in thickness, perpendicular to the longitudinal axis. Some ventricular rings were prepared for assay of oxidative stress biomarker (malondialdehyde, MDA).^[11] 10% neutral buffered formalin (NBF) was used to fix specimens from both the left ventricle and the right atrium and then processed to obtain paraffin sections for light microscopic study. A transmission electron microscope (TEM) analysis was conducted on fine samples (~ 1 mm³) obtained from the left ventricle and the right atrium in each group.

Light microscopic study

Specimens taken from the left ventricle and the right atrium were fixed in 10% NBF. This was followed by dehydration in ascending grades of alcohol and clearance in xylene. Paraffin sections (4-5 µm thick) were prepared. The sections were stained with Hematoxylin and Eosin stain (H & E)^[12] for routine histological analysis, Masson's Trichrome stain^[12] for illustration of collagenous fibers, and immunohistochemical stains^[13]: caspase-3 immunostaining as a marker for apoptosis^[14] and CD117 (C-kit) immunostaining as a marker for cardiac stem cells (CSCs).^[15]

Procedure of immunohistochemistry of caspase-3 and CD117 (C-kit)

Paraffin sections (4-5 µm thick) were cut and placed on coated slides for immunohistochemical analysis using the avidin-biotin–complex (ABC) immunoperoxidase technique. The slides were placed in hydrogen peroxide for 10 minutes to inhibit the endogenous activity of peroxidase. After that, phosphate buffered saline (PBS) solution was utilized for washing the slides for ten minutes. The slides were initially placed in citrate buffer with a (pH=6) and then boiled for 10 minutes at 100°C in a microwave oven to expose the antigenic peptide and perform antigen retrieval. After that, the sections were incubated for 90 min at room temperature with the primary antibodies, anti-caspase-3 (diluted at 1:500) and anti-CD117 (C-kit) (diluted at 1:500). The primary antibodies were identified using an anti-rabbit secondary antibody. The biotinylated secondary antibody was added in two drops. The slides were incubated in bovine serum albumin (1%; 1/200 concentration) dissolved in PBS for 10 minutes at room temperature to avoid nonspecific background staining. The staining process was completed when the reaction site produced a brown precipitate following a 5 to 10-minute incubation period with the substrate chromogen, DAB

(3,30 Diaminobenzidine). The counterstain employed was Mayer's Hematoxylin.^[16] Sections of (lymph node for caspase-3^[17] and GIST (gastrointestinal stromal tumor) for CD117 (C-kit)^[18]) were used as positive tissue control in order to assess the reagents' effectiveness (Figures 1 A,C). Tissue sections were additionally provided with negative control slides, where no primary antibodies were utilized, to evaluate the background staining. The absence of primary antibody cross reactivity is verified by the negative control slide which lacked specific staining (Figures 1 B,D).

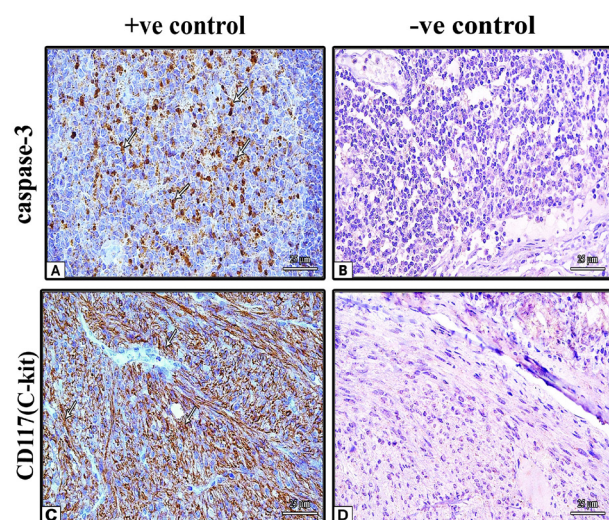


Fig. 1: Photomicrographs of positive and negative tissue controls. (A) lymph node of a control rat used as a positive control for caspase-3 showing positive immune reaction in the form of brown color (arrows). (B) a section of the lymph node used as a negative control slide showing negative immune reaction for caspase-3. (C) Gastrointestinal stromal tumor (GIST) tissue used as a positive control for CD117 (C-kit) showing positive immune reaction in the form of brown color in interstitial cells of Cajal (arrows). (D) a section of GIST tissue used as a negative control slide showing negative immune reaction for CD117. (A and B) IHC for caspase-3 \times 400, (C and D) IHC for CD117 \times 400).

Electron microscopic study

0.1 M phosphate buffer with a (pH=7.4) (that contained 2.5% of glutaraldehyde and 2% of paraformaldehyde) was used to fix tiny samples (less than 1 mm³) from the left ventricle and the right atrium from all groups overnight. Following a one-hour postfixation in osmium tetroxide (1%) at temperature of 4°C, the specimens were washed three rounds in PBS for ten minutes each. Toluidine blue was utilized for staining semithin sections that were one micrometer thick to examine the cardiac muscle and determine the appropriate locations for ultrathin sectioning. Lead citrate and uranyl acetate were utilized to stain ultrathin sections (60–80 nm) for ten minutes each^[19]. Ultrathin sections were examined using JEOL JEM-2100 transmission electron microscope (TEM) running at 160 Kilovolt at the Electron Microscopic Unit in Faculty of Agriculture, Mansoura University.

Biochemical study

Left ventricular specimens from all groups were

weighed and homogenized using a Potter-Elvehjem tissue homogenizer in 10 mM of potassium phosphate buffer with a (pH=7.4) to estimate the amount of malondialdehyde (MDA) (an oxidative stress indicator) in the cardiac tissue homogenate. The crude tissue homogenate was centrifuged for 15 minutes at 10,000 rotations per minute (rpm). Using the obtained supernatant, MDA was estimated^[20] utilizing commercial assay kit (catalog number: RC0011) obtained from Medaysis Company. Samples taken from the supernatant were kept at 4°C until their MDA levels were measured.^[11]

Histomorphometric study and image analysis using ImageJ version (1.52a)

The area percentage of collagenous fibers in the endomysium present among the cardiac muscle fibers and in the perivascular areas was measured in sections stained with Masson's trichrome stain. The area percentage and the mean number of caspase-3 and CD117 (C-Kit) immunopositive cells were measured in immunohistochemically stained slides. Six distinct non-overlapping randomly chosen fields from the cardiac muscle fibers at a magnification of 400 were examined on six slides from every group to calculate the morphometric data. An Olympus E420 digital camera was used to capture photos of the slides. It was attached to an Olympus microscope that had a 40 \times objective lens (TX31 Philippines) and a 0.5 \times photo adaptor. After that, ImageJ program was used to analyze the images.

Statistical study

Version 17.0 of SPSS program (Statistical Package for Social Science) was utilized to tabulate, code, and analyze the results including the MDA level and the histomorphometric data. Mean \pm standard deviation (\pm SD) was utilized to represent the data. More than two sets of numerical (parametric) data were compared using one-way ANOVA test. The post-hoc Tukey test was used for several comparisons.^[21] *P* value was regarded as statistically significant if it was less than 0.05. N.B: there was a blinded statistical evaluation. The study layout and study groups were unknown to the microscopists and analysts.

RESULTS

Animals

All animals in all groups were alive and in a good general condition till the end of experiment (No dead animals).

Light microscopic results

Regarding H&E, Masson's trichrome, and anti-caspase-3 stains, there was no significant difference between the left ventricle and the right atrium in all groups. Therefore, our results are represented with the left ventricle.

H&E Stain

Group I (Control group): The longitudinal sections of the cardiac muscle fibers of the left ventricle had central oval vesicular nuclei and acidophilic cytoplasm. Darkly stained intercalated discs were observed. The transverse sections of the muscle fibers appeared polyhedral with acidophilic cytoplasm and central vesicular nuclei. Fibroblasts and normal blood capillaries were seen in the endomysium among the muscle fibers (Figures 2 A,B).

Group II (HFD group): Left ventricular sections of HFD group exhibited areas of myocardial damage. Marked disorganization and disruption of the cardiac muscle fibers were observed. The fibers were widely spaced and showed cytoplasmic vacuolations. Some fibers showed homogenous intensely stained acidophilic cytoplasm and shrunken deeply stained peripheral nuclei. Other fibers showed shrunken nuclei with perinuclear halos (Figures 2 C,D).

Group III (HFD + G-CSF group): Left ventricular sections of HFD + G-CSF group revealed partial restoration of the cardiac muscle fiber organization. Disruption of the muscle fibers and wide spacing were not remarkable. Few fibers showed intensely stained acidophilic cytoplasm and small deeply stained peripheral nuclei. Few cytoplasmic vacuolations were seen in some fibers (Figures 2 E,F).

Masson 's trichrome stain

Group I (Control group): Fine collagenous fibers were seen in the endomysium among the cardiac muscle fibers and around the blood vessels in both longitudinal and transverse left ventricular sections of the control group (Figures 3 A,B).

Group II (HFD group): Evident deposition of collagenous fibers was detected in the endomysium and in the perivascular areas in both longitudinal and transverse left ventricular sections of HFD group (Figures 3 C,D).

Group III (HFD + G-CSF group): Mild deposition of collagenous fibers was observed in the endomysium and in the perivascular areas in both longitudinal and transverse left ventricular sections of HFD + G-CSF group (Figures 3 E,F).

Results of immunohistochemistry**Immune expression of Caspase-3**

Group I (Control group): Minimal cytoplasmic immune expression of caspase-3 was detected in both longitudinal and transverse left ventricular sections of the control group (Figures 4 A,B).

Group II (HFD group): There was positive cytoplasmic and nuclear immune expression of caspase-3 in the majority of the cardiac muscle fibers in both longitudinal and transverse left ventricular sections of HFD group (Figures 4 C,D).

Group III (HFD + G-CSF group): Positive cytoplasmic

immune expression of caspase-3 appeared in few fibers in both longitudinal and transverse left ventricular sections of HFD + G-CSF group (Figures 4 E,F).

Immune expression of CD117 (C-kit)

There was structural difference between the left ventricle and the right atrium in all groups. Therefore, our results are represented separately in both the left ventricle and the right atrium.

1- Left ventricular sections

Group I (Control group): showed cells with positive cytoplasmic immune expression of CD117 among the cardiac muscle fibers in both longitudinal and transverse sections (Figures 5 A,B).

Group II (HFD group): showed cells with positive cytoplasmic immune expression of CD117 among the cardiac muscle fibers in both longitudinal and transverse sections (Figures 5 C,D).

Group III (HFD + G-CSF group): showed cells with positive cytoplasmic immune expression of CD117 among the cardiac muscle fibers in both longitudinal and transverse sections (Figures 5 E,F). The reaction was apparently increased in comparison with both the control group and HFD group.

2- Right atrial sections

Group I (Control group): showed cells with positive cytoplasmic immune expression of CD117 among the cardiac muscle fibers in both longitudinal and transverse sections (Figures 6 A,B). When compared to the left ventricular sections in the control group, the reaction was comparatively increased.

Group II (HFD group): showed cells with positive cytoplasmic immune expression of CD117 among the cardiac muscle fibers in both longitudinal and transverse sections (Figures 6 C,D).

Group III (HFD + G-CSF group): showed cells with positive cytoplasmic immune expression of CD117 among the cardiac muscle fibers in both longitudinal and transverse sections (Figures 6 E,F). In comparison to the control group and HFD group, upregulation of CD117 immune expression was observed.

Electron microscopic results**1- Left ventricular ultrathin sections**

Group I (Control group): showed regularly arranged myofibrils with well-organized sarcomeres extending between two Z lines. The mitochondria were packed in longitudinal rows between the myofibrils (Intermyofibrillar mitochondria) (IMFM). The cardiac myocyte had oval euchromatic nucleus. Perinuclear mitochondria (PNM) were seen at the pole of the nucleus (Figure 7A). The myofibrils showed the regular banding and normal striation pattern with dark (A) bands and light (I) bands alternate with each other. Darkly stained Z lines bisected

the light bands. H zones were also seen as lightly stained zones in the center of the dark bands. Electron dense glycogen granules were detected in the interfibrillar spaces. T-tubule (transverse tubule) of the sarcomeric diad was also observed at the level of the Z line of the sarcomere (Figure 7B). Intercalated discs between the cardiac myocytes acquired a zigzag-like appearance with fascia adherens and desmosomes in the transverse parts and gap junctions in the longitudinal parts (Figure 7C). The endomysium showed a little amount of collagen fibrils and blood capillaries (Figure 7D).

Group II (HFD group): showed marked ultrastructural degenerative alterations. Aggregations of variable-sized lipid droplets were seen in the perinuclear area (Figure 8A) and between the myofibrils (Figure 8B). The lipid droplets were electron lucent. Marked disorganization and disruption of the myofibrils were observed (Figures 8 B,C). Mitochondria were irregularly arranged with variable sizes and abnormal shapes (Figures 8 B,C). Intercalated disc displayed irregularity and widening (Figure 8C). Secondary lysosomes were also seen (Figure 8C). Marked collagen deposition was demonstrated in the endomysium. Irregularity and scalloping of the sarcolemma and subsarcolemmal accumulation of swollen mitochondria were observed (Figure 8D).

Group III (HFD + G-CSF group): demonstrated partial improvement. The myofibrils were relatively organized compared with HFD group. However, focal areas of myofibrillar disruption were detected. The nucleus of the cardiac myocyte appeared euchromatic. Mitochondria appeared relatively normal (Figure 9A). Fewer and smaller lipid droplets were seen between the myofibrils (Figure 9B) in comparison to HFD group. Intercalated discs appeared normal (Figure 9C) as compared with HFD group. The endomysium showed relatively little amount of collagen (Figure 9D) as compared with HFD group.

2- Right atrial ultrathin sections

Group I (Control group): The cardiac myocytes showed electron dense granules of atrial natriuretic peptide. The endomysium showed an ovoid stem cell with ovoid euchromatic nucleus and a triangular telocyte with euchromatic nucleus and telocyte processes (telopodes) (Figure 10A).

Group II (HFD group): The cardiac myocyte revealed shrunken heterochromatic nucleus and electron dense granules of atrial natriuretic peptide at one pole of the nucleus. The endomysium showed a stem cell with euchromatic nucleus, scattered mitochondria, and short cytoplasmic processes. A telocyte with condensed irregular nucleus, cytoplasmic vacuolations, and telopodes was also demonstrated (Figure 10B).

Group III (HFD + G-CSF group): The cardiac myocytes showed well-organized myofibrils with variable-sized electron dense atrial natriuretic granules. The endomysium showed stem cells with oval euchromatic

nuclei and triangular telocytes with euchromatic nuclei and their telopodes. Rounded variable-sized cytoplasmic vacuolations appeared in some telocytes (Figures 10 C,D).

Statistical results

Malondialdehyde (MDA) level in the cardiac tissue homogenates (nmol/g. tissue)

When compared to the control group "group I", the mean level of MDA in the cardiac tissue homogenates of the HFD group "group II" increased significantly ($P < 0.05$). However, this level was significantly lower ($P < 0.05$) in the HFD + G-CSF group "group III" than in the HFD group, but it was still significantly greater ($P < 0.05$) than in the control group (Table 1).

Image analysis results

Area percentage of the collagenous fibers in sections stained with Masson's trichrome /high-power field (X400)

The mean area percentage of the collagenous fibers in the HFD group "group II" increased significantly ($P < 0.05$) in comparison to the control group "group I". On the other hand, this percentage in the HFD + G-CSF group "group III" was significantly lower ($P < 0.05$) than in the HFD group, but it was still significantly higher ($P < 0.05$) than in the control group (Table 2).

Area percentage of positive immune expression of caspase-3 in caspase-3 immunohistochemically-stained sections /high-power field (X400)

The HFD group "group II" had a significantly higher ($P < 0.05$) mean area percentage of positive immune expression of caspase-3 than the control group "group I." However, this percentage in the HFD + G-CSF group "group III" was significantly lower ($P < 0.05$) than in the HFD group, but it was still significantly higher ($P < 0.05$) than in the control group (Table 3).

Area percentage of positive immune expression of CD117 in CD117 immunohistochemically-stained left ventricular sections /high-power field (X400)

The mean area percentage of positive immune expression of CD117 in left ventricular sections of the HFD group "group II" increased non-significantly ($P = 0.805$) in comparison to the control group "group I". Moreover, this percentage in left ventricular sections of the HFD + G-CSF group "group III" increased significantly ($P < 0.05$) in comparison to the HFD group and the control group (Table 4).

Area percentage of positive immune expression of CD117 in CD117 immunohistochemically-stained right atrial sections /high-power field (X400)

In the right atrial sections of the HFD group "group II", the mean area percentage of positive immune expression of CD117 was non-significantly higher ($P = 0.295$) than in the control group "group I". Moreover, the right atrial sections of the HFD + G-CSF group "group III" exhibited

a significantly higher percentage ($P < 0.05$) in comparison to the HFD group and the control group (Table 5).

Mean number of immuno-positive cells for caspase-3 in caspase-3 immunohistochemically-stained sections / high-power field (X400)

The mean number of immuno-positive cells for caspase-3 in the HFD group "group II" was significantly greater ($P < 0.05$) than in the control group. However, this number was significantly lower ($P < 0.05$) in the HFD + G-CSF group "group III" than in the HFD group, but it was still significantly higher ($P < 0.05$) than in the control group (Table 6).

Mean number of immuno-positive cells for CD117 in CD117 immunohistochemically-stained left ventricular sections /high-power field (X400)

The mean number of immuno-positive cells for CD117

in left ventricular sections of the HFD group "group II" increased, but not significantly ($P = 0.204$) when compared to the control group. In addition, this number in the HFD + G-CSF group "group III" was significantly greater ($P < 0.05$) than in the HFD group and the control group (Table 7).

Mean number of immuno-positive cells for CD117 in CD117 immunohistochemically-stained right atrial sections /high-power field (X400)

The mean number of immuno-positive cells for CD117 in right atrial sections of the HFD group "group II" was non-significantly higher ($P = 0.248$) than in the control group. Moreover, this number in the HFD + G-CSF group "group III" was significantly greater ($P < 0.05$) than in the HFD group and the control group (Table 8).

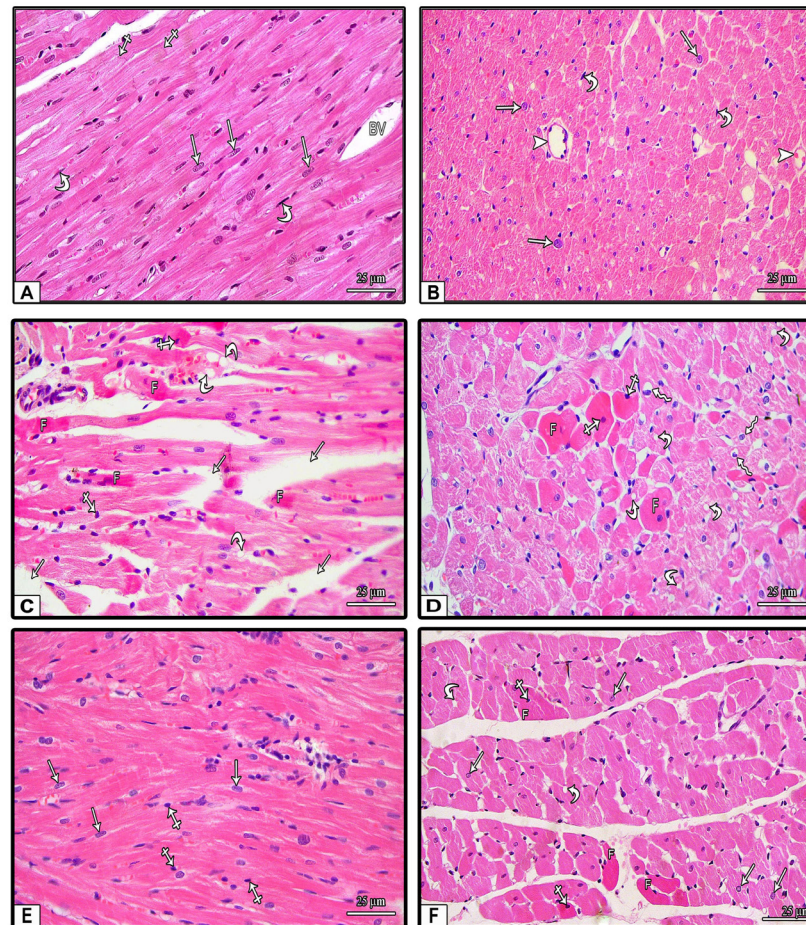


Fig. 2: Photomicrographs of paraffin sections in the left ventricle of all groups: (A, B) sections from group I (control group). (A) shows longitudinally cut cardiac muscle fibers with central, oval, and vesicular nuclei (arrows). Darkly stained intercalated discs (crossed arrows) are observed. Non-congested blood vessel (BV) and fibroblasts (curved arrows) are demonstrated in the endomysium. (B) shows transversely cut muscle fibers which appear polyhedral with mostly central vesicular nuclei (arrows). The endomysium contains fibroblasts (curved arrows) and normal blood capillaries (arrowheads). (C, D) longitudinal and transverse sections from group II (HFD group) respectively. (C) shows areas of disorganization, spacing, and disruption (arrows) of the muscle fibers. (C, D) show homogenous intensely stained acidophilic cytoplasm and shrunken deeply stained peripheral nuclei (crossed arrows) in some fibers (F). Cytoplasmic vacuolations (curved arrows) are also seen in some fibers. Other fibers show shrunken nuclei with perinuclear halos (zigzag arrows). (E, F) sections from group III (HFD+G-CSF group). (E) shows longitudinally cut muscle fibers which appear relatively normal with oval, vesicular, and central nuclei (arrows). Few fibers show small darkly stained peripheral nuclei (crossed arrows). (F) shows transversely cut muscle fibers which appear polyhedral with central vesicular nuclei (arrows). Few fibers (F) have intensely stained acidophilic cytoplasm and small deeply stained peripheral nuclei (crossed arrows). Other fibers show cytoplasmic vacuolations (curved arrows). (H & E X 400).

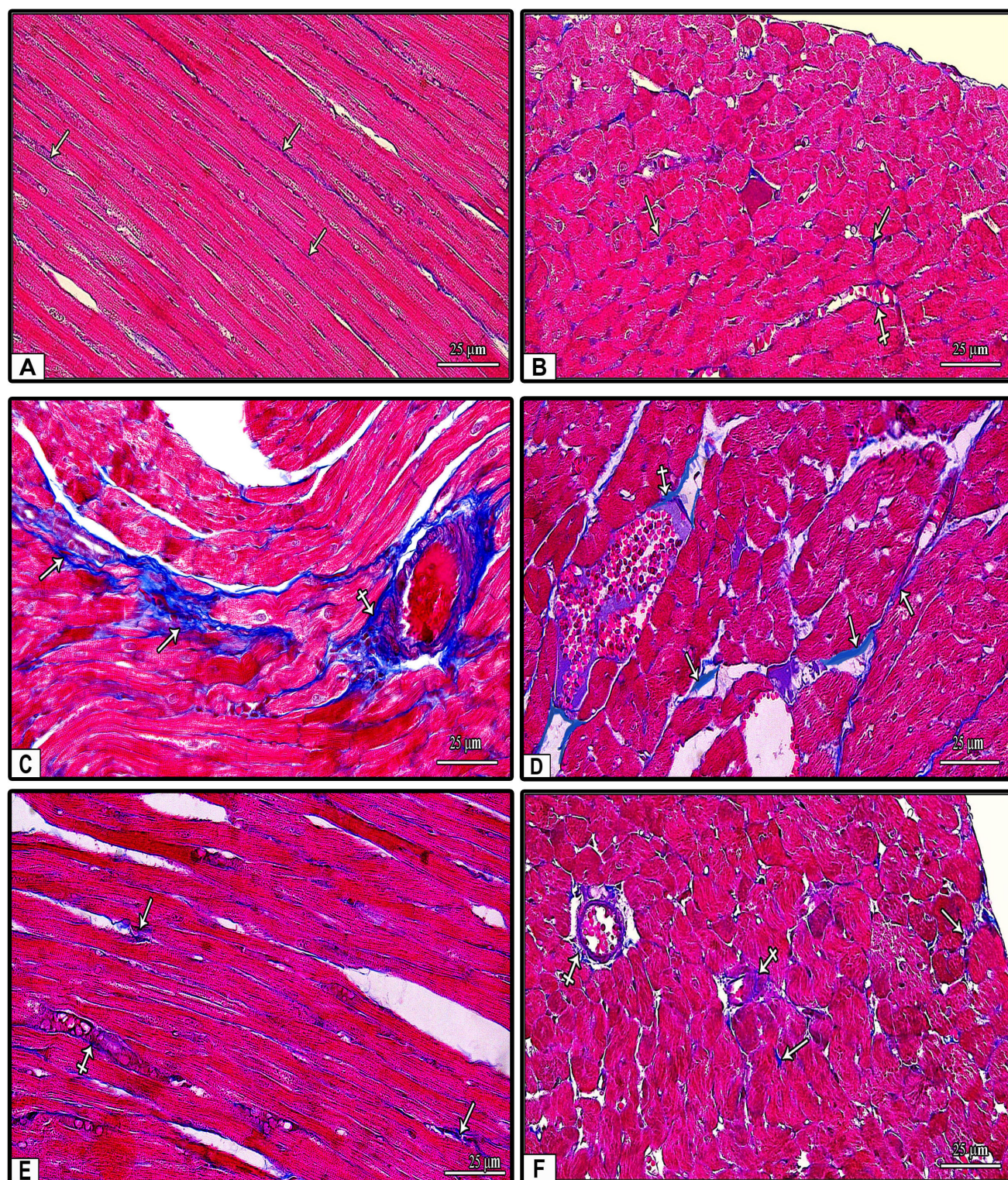


Fig. 3: Photomicrographs of paraffin sections in the left ventricle of all groups: (A, B) longitudinal and transverse sections from group I (control group) respectively, showing fine collagenous fibers in the endomysium (arrows) among the muscle fibers and around blood vessels (crossed arrow). (C, D) longitudinal and transverse sections from group II (HFD group) respectively, showing evident deposition of collagenous fibers in the endomysium (arrows) among the muscle fibers and in the perivascular areas (crossed arrows). (E, F) longitudinal and transverse sections from group III (HFD+G-CSF group) respectively, showing mild deposition of collagenous fibers in the endomysium (arrows) among the muscle fibers and in the perivascular areas (crossed arrows). (Masson's trichrome X 400).

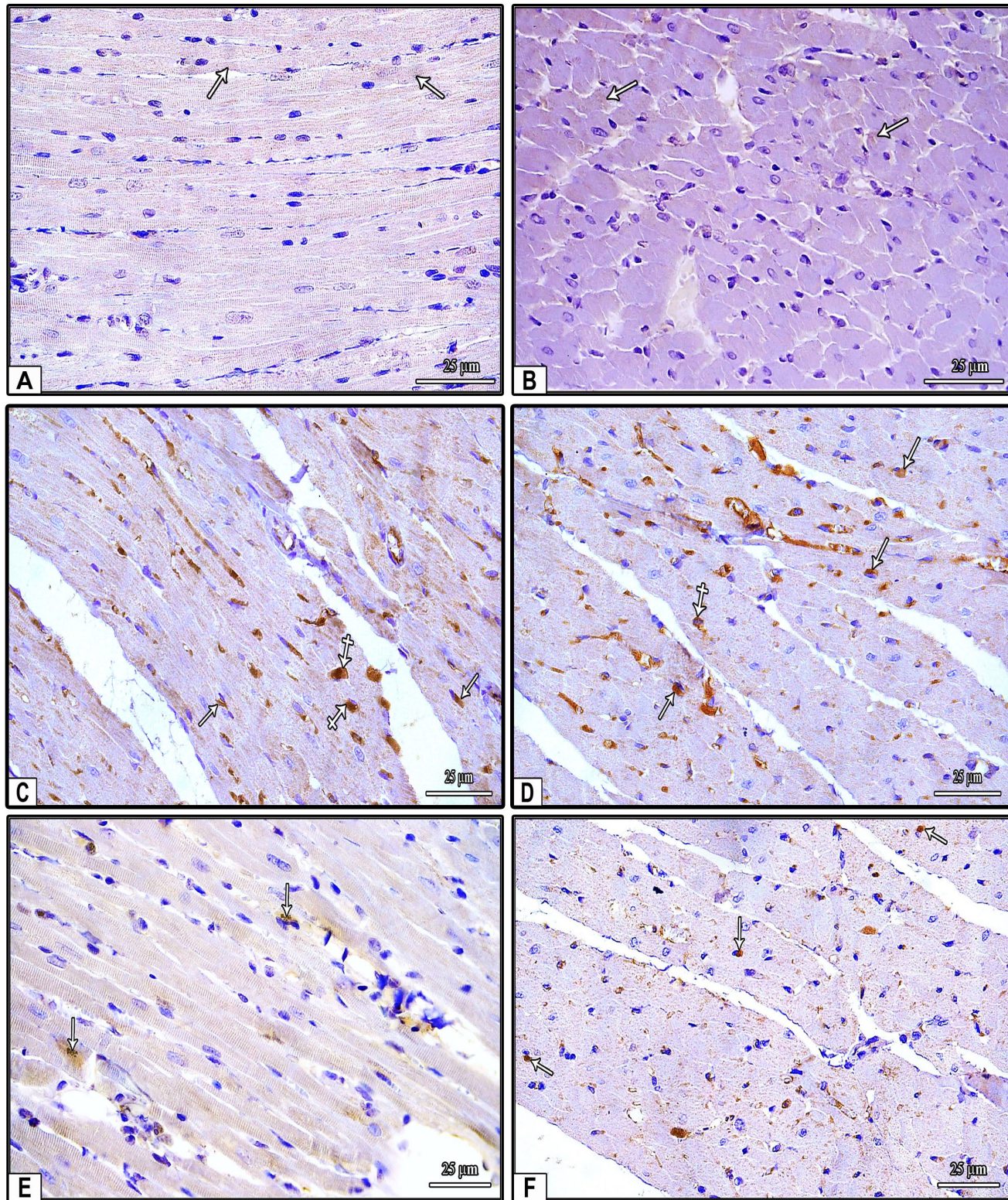


Fig. 4: Photomicrographs of paraffin sections in the left ventricle of all groups showing caspase-3 immune reaction: (A, B) longitudinal and transverse sections from group I (control group) respectively, showing minimal cytoplasmic immune reaction of caspase-3 (arrows). (C, D) longitudinal and transverse sections from group II (HFD group) respectively, showing positive caspase-3 immune reaction in the cytoplasm (arrows) or in both the cytoplasm and nuclei (crossed arrows) of the majority of the cardiac muscle fibers. (E, F) longitudinal and transverse sections from group III (HFD+G-CSF group) respectively, showing positive caspase-3 immune reaction in the cytoplasm (arrows) of few cardiac muscle fibers. (IHC for caspase-3 x 400).

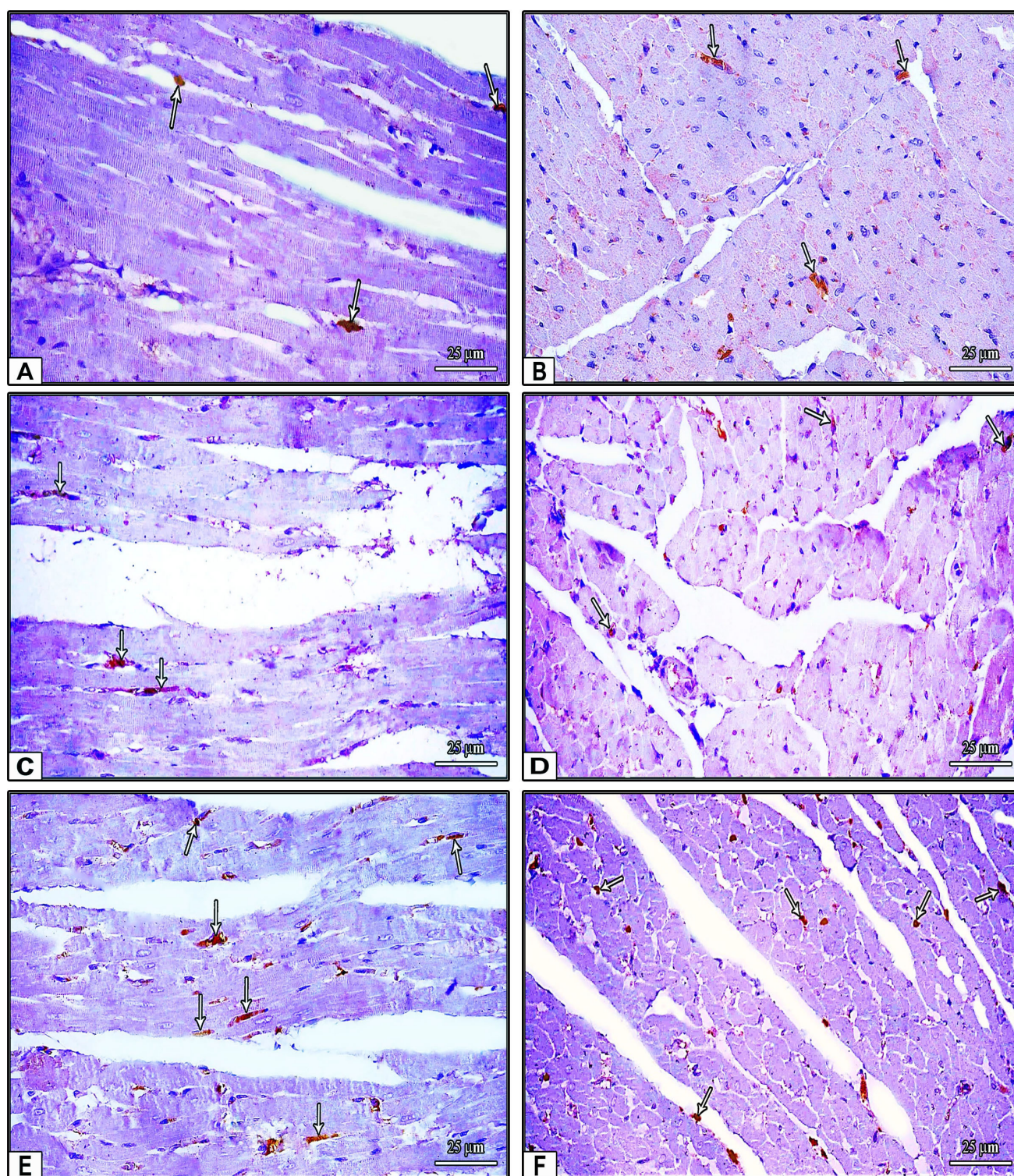


Fig. 5: Photomicrographs of paraffin sections in the left ventricle of all groups showing CD117 (C-kit) immune reaction: (A, B) longitudinal and transverse sections from group I (control group) respectively, showing positive cytoplasmic immune reaction of CD117 +ve cells (arrows) among the cardiac muscle fibers. (C, D) longitudinal and transverse sections from group II (HFD group) respectively, showing positive cytoplasmic immune reaction of CD117 +ve cells (arrows) among widely spaced cardiac muscle fibers. (E, F) longitudinal and transverse sections from group III (HFD+G-CSF group) respectively, showing positive cytoplasmic immune reaction of CD117 +ve cells (arrows) among the cardiac muscle fibers. Note, the apparent increase in immune reaction in comparison to both the control group and HFD group. (IHC for CD117 x 400).

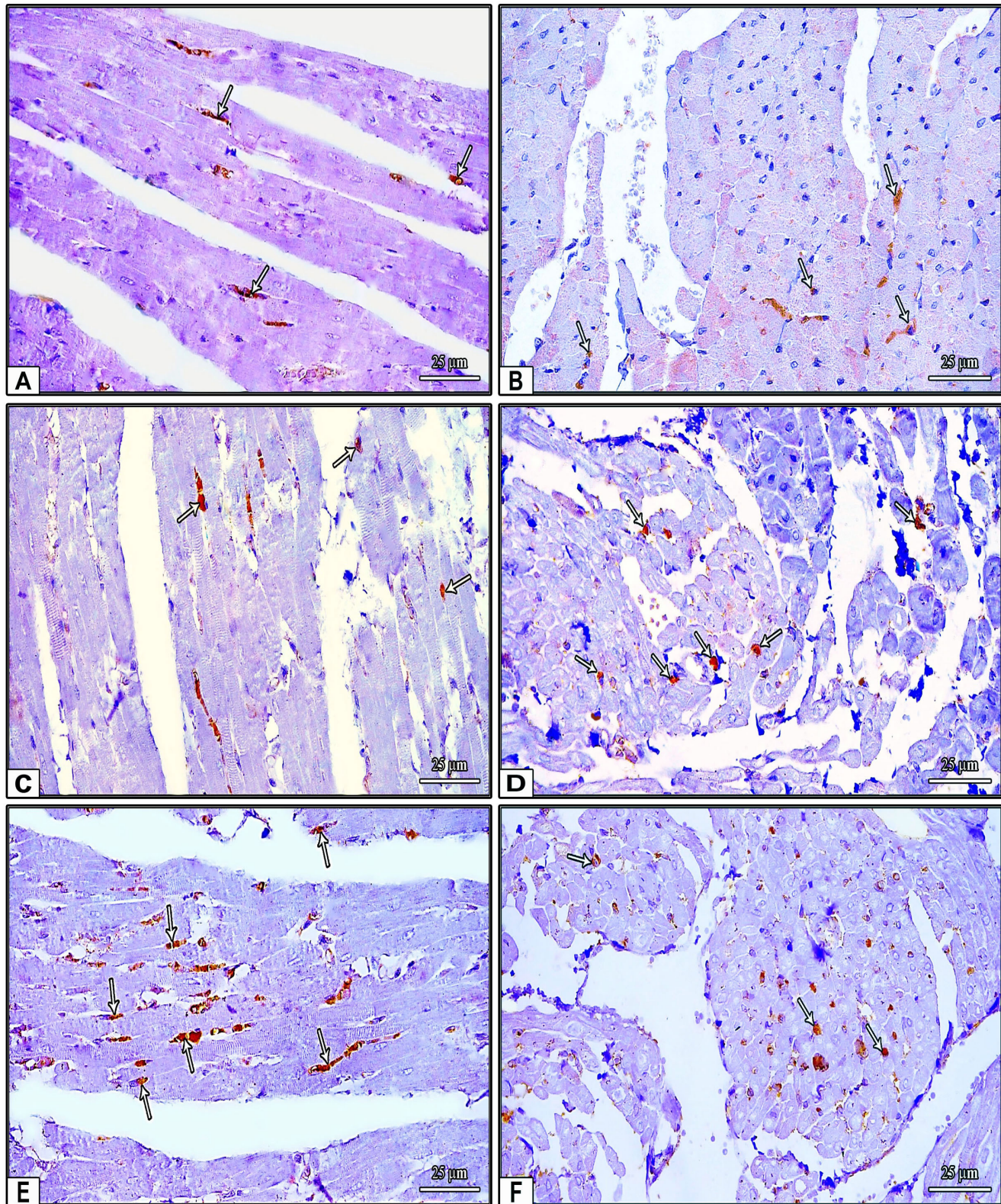


Fig. 6: Photomicrographs of paraffin sections in the right atrium of all groups showing CD117 (C-kit) immune reaction: (A, B) longitudinal and transverse sections from group I (control group) respectively, showing positive cytoplasmic immune reaction of CD117 +ve cells (arrows) among the cardiac muscle fibers. Note, the relatively increased CD117 immune reaction in comparison to the left ventricular sections of the control group. (C, D) longitudinal and transverse sections from group II (HFD group) respectively, showing positive cytoplasmic immune reaction of CD117 +ve cells (arrows) among the cardiac muscle fibers. Note, the relative increase in number of positive cells in comparison to the control group. (E, F) longitudinal and transverse sections from group III (HFD+G-CSF group) respectively, showing positive cytoplasmic immune reaction of CD117 +ve cells (arrows) among the cardiac muscle fibers. Note, the apparent increase in immune reaction in comparison to both the control group and HFD group. (IHC for CD117 x 400).

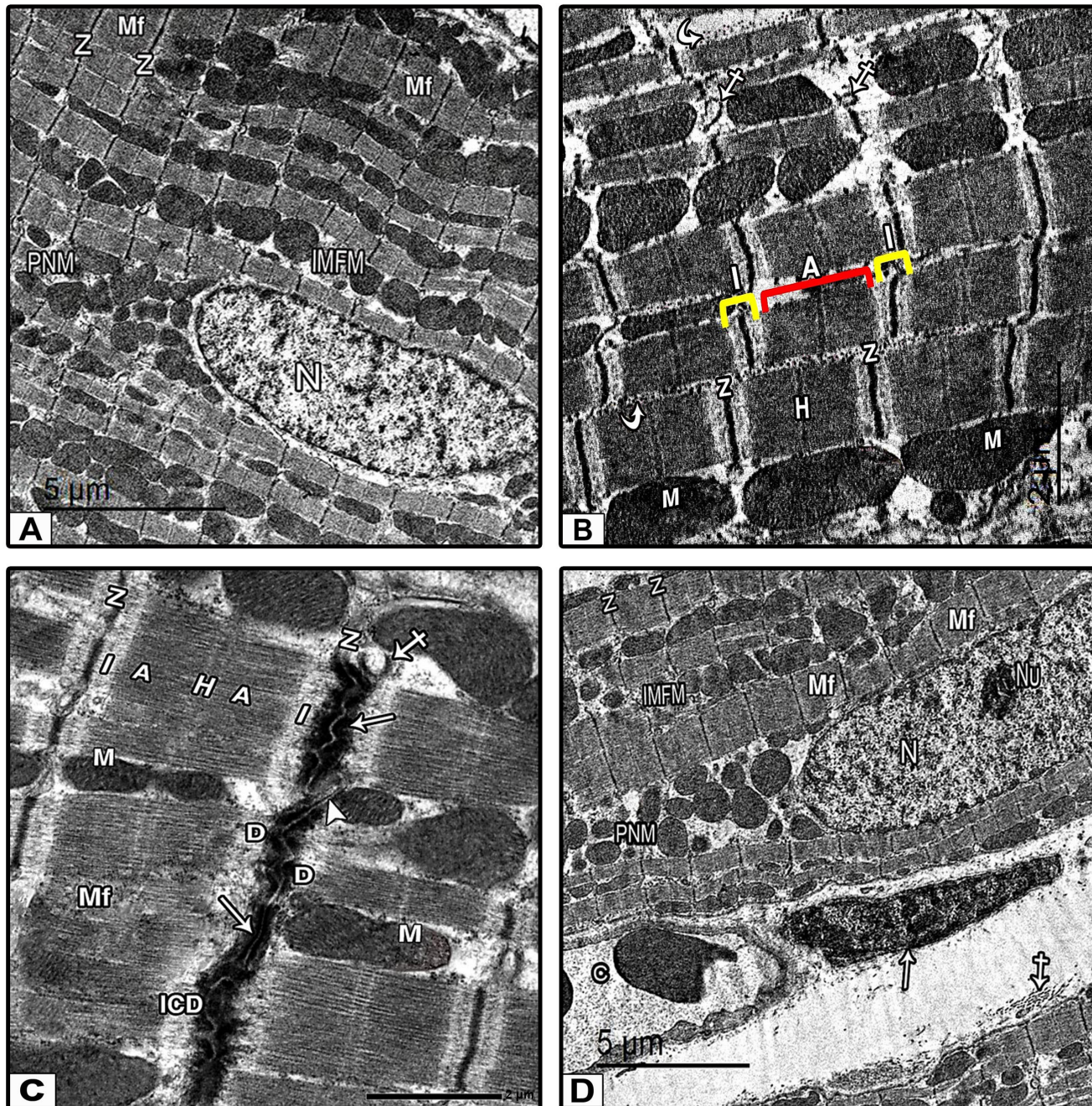


Fig. 7: Electron micrographs in the left ventricle of group I (control group). (A) shows regularly arranged myofibrils (Mf) with well-organized sarcomeres extending between two Z lines (Z). The mitochondria are packed in longitudinal rows between the myofibrils (Intermyofibrillar mitochondria) (IMFM). The cardiac myocyte has oval and euchromatic nucleus (N). Perinuclear mitochondria (PNM) are seen at the pole of the nucleus. (B, C) show well-organized myofibrils with alternating dark (A) bands (red bracket) and light (I) bands (yellow brackets). Z lines (Z) and H zones (H) are demonstrated. Mitochondria (M) are arranged in rows between the myofibrils. Note, the electron dense glycogen granules (curved arrows) in intermyofibrillar spaces and the T-tubule (crossed arrows) at the level of Z lines. In Fig. (C) shows zigzag-like intercalated disc (ICD). It is formed of fascia adherens (arrows), desmosomes (D) and gap junctions (arrowhead). In Fig. (D), the nucleus of the cardiac myocyte has a prominent nucleolus (Nu). The endomysium reveals spindle-shaped fibroblast (arrow), little amount of collagen fibrils (crossed arrow), and a blood capillary (C). (TEM A x 1200, B x 2000, C x 3000, D x 1000).

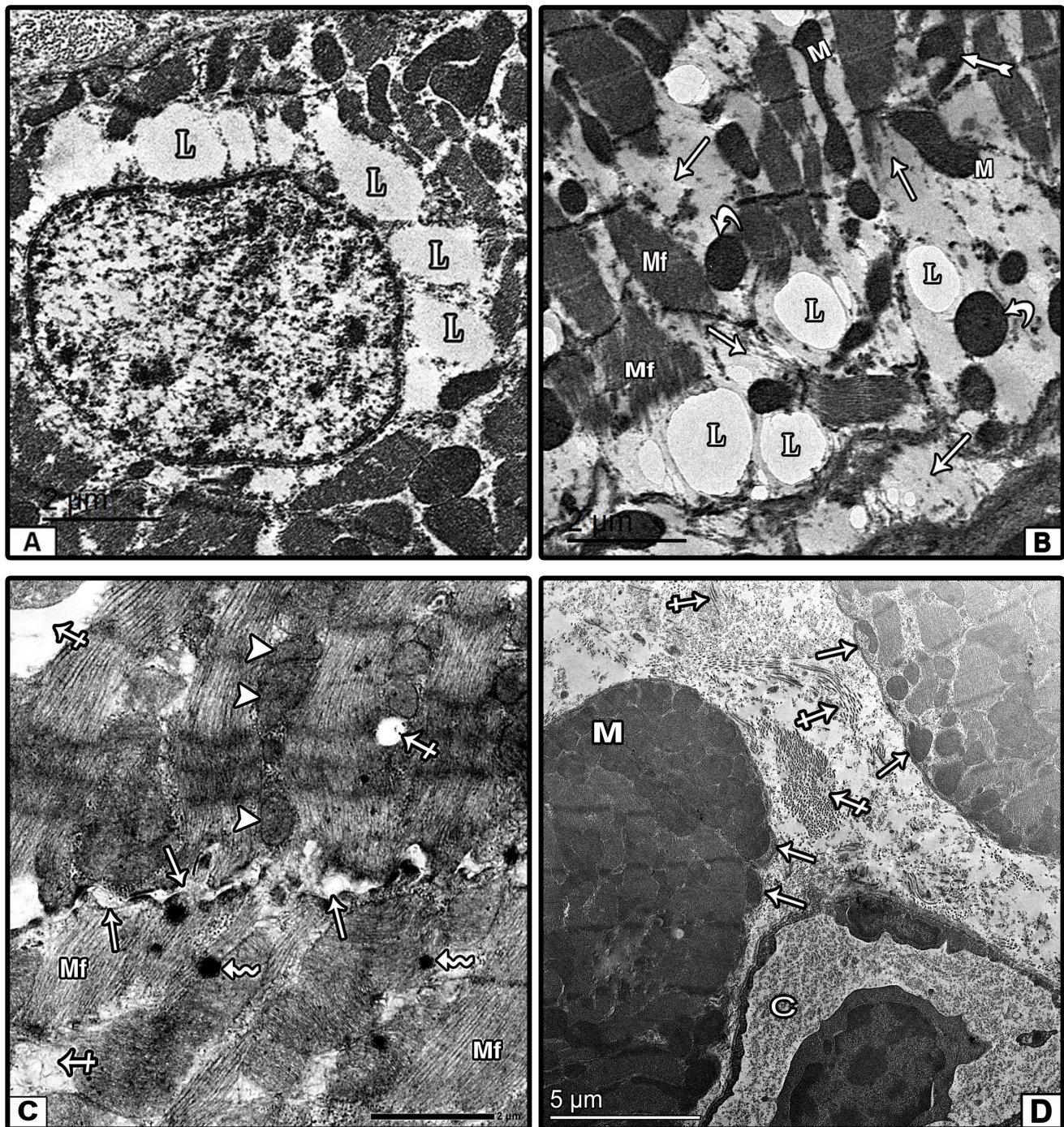


Fig. 8: Electron micrographs in the left ventricle of group II (HFD group). (A) shows variable-sized lipid droplets (L) in the perinuclear area of the cardiac myocyte. (B) shows marked disorganization of the myofibrils (Mf) and marked myofibrillar loss and disruption (arrows). The mitochondria are irregularly arranged. Some mitochondria show marked electron dense matrix (curved arrows), others are bizarre-shaped (M) or crescent-shaped (bifid arrow). Scattered variable-sized lipid droplets (L) appear between the myofibrils. (C) shows irregularity and widening of the intercalated disc (arrows). Swollen mitochondria (arrow heads), areas of myofibrillar disruption (crossed arrows), and secondary lysosomes (zigzag arrows) are demonstrated. (D) shows marked collagen deposition (crossed arrows) and a blood capillary (C) in the endomysium. Scalloping of the sarcolemma (arrows) and aggregated swollen subsarcolemmal mitochondria (M) are demonstrated. (TEM A x 2000, B x 2000, C x 3000, D x 1000).

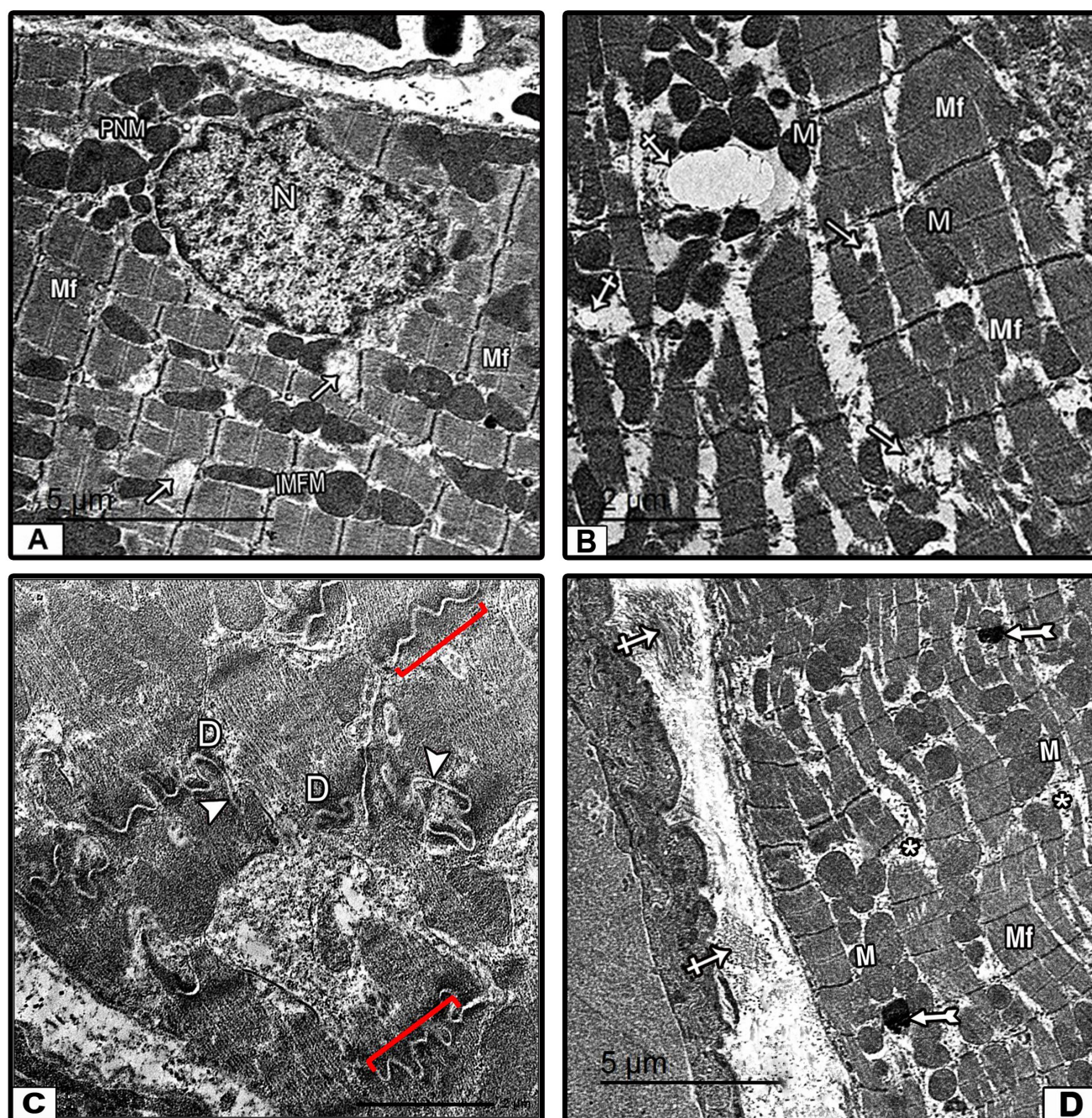


Fig. 9: Electron micrographs in the left ventricle of group III (HFD+G-CSF group). (A) shows relatively organized myofibrils (Mf) and regularly arranged myofilaments with the normal striation pattern. Focal areas of myofibrillar disruption (arrows) are demonstrated. Mitochondria are arranged in longitudinal rows between the myofibrils (Intermyofibrillar mitochondria) (IMFM). The nucleus (N) is euchromatic. Perinuclear mitochondria (PNM) are seen at the pole of the nucleus. (B) shows relatively organized myofibrils (Mf) with relatively fewer and smaller lipid droplets (crossed arrows) between the myofibrils. Mitochondria (M) have variable sizes, shapes, and distribution. Focal disruption of the myofilaments (arrows) is demonstrated. (C) shows normal intercalated discs which are formed of fascia adherens (red brackets), desmosomes (D), and gap junctions (arrow heads). (D) shows relatively organized myofibrils (Mf) with some areas of disruption (asterisks). The intermyofibrillar mitochondria (M) appear relatively normal. Secondary lysosomes (bifid arrows) are demonstrated. The endomysium shows collagen deposition (crossed arrows) which is relatively little in amount as compared to Fig. 8D. (TEM A x 1500, B x 2000, C x 3000, D x 1200).

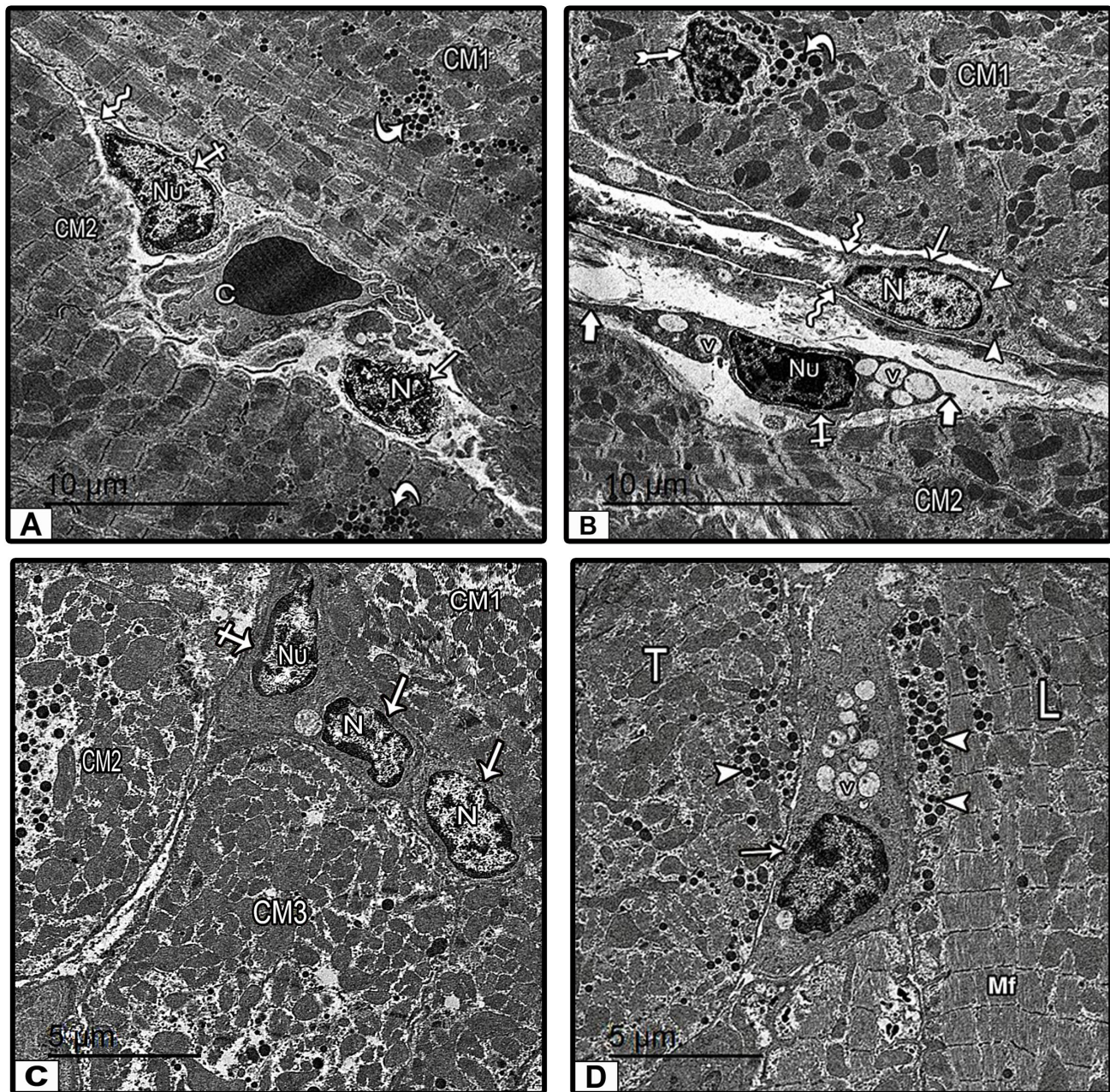


Fig. 10: Electron micrographs in the right atrium of all groups. (A) a section from group I (control group) shows two cardiac myocytes (CM1, CM2) with the C.T. endomysium. The endomysium shows an ovoid stem cell (arrow) with ovoid euchromatic nucleus (N) and a triangular telocyte (crossed arrow) with euchromatic nucleus (Nu) and a telopode (zigzag arrow). Both the stem cell and the telocyte are situated near a blood capillary (C). Note, presence of electron dense atrial natriuretic granules (curved arrows) in the cardiac myocytes. (B) a section from group II (HFD group) shows two cardiac myocytes (CM1, CM2) with the C.T. endomysium. The endomysium shows a stem cell (arrow) with oval euchromatic nucleus (N), scattered mitochondria (arrow heads), and short cytoplasmic processes (zigzag arrows). A telocyte (crossed arrow) with condensed irregular nucleus (Nu), cytoplasmic vacuolations (V), and telopodes (thick arrows) is demonstrated. CM1 shows a shrunken heterochromatic nucleus (bifid arrow) and electron dense granules of atrial natriuretic peptide (curved arrow) at one pole of the nucleus. (C) a section from group III (HFD+G-CSF group) shows three cardiac myocytes (CM1, CM2, CM3) with the C.T. endomysium. The endomysium shows two stem cells (arrows) with ovoid euchromatic nuclei (N) and a telocyte (crossed arrow) with ovoid euchromatic nucleus (Nu). (D) a section from group III (HFD+G-CSF group) shows a longitudinal cardiac myocyte (L) and a transverse one (T). The myofibrils (Mf) are well-organized with variable-sized electron dense atrial natriuretic granules (arrow heads). A triangular telocyte (arrow) with variable-sized cytoplasmic vacuolations (V) is demonstrated in the endomysium. (TEM A and B x 800, C and D x 1000).

Table 1: Malondialdehyde (MDA) level (nmol/g. tissue) in the cardiac tissue homogenates within study groups (Mean \pm SD)

	Control Group (Group I) (N=10)	HFD Group (Group II) (N=10)	HFD + G-CSF Group (Group III) (N=10)	Significance test
Mean \pm SD	48.53 \pm 4.69	117.1 \pm 7.24	83.25 \pm 6.51	
P1		0.001<*	0.001<*	One-way ANOVA
P2			0.001<*	<i>P value</i> 0.001<*

Note: N: number, SD: standard deviation, P: Probability of ANOVA.

* : statistically significant ($P \leq 0.05$).

P1: Significance in relation to group I (control group) P2: Significance in relation to group II (HFD group).

Table 2: Area percentage of the collagenous fibers /HPF (X400) within study groups (Mean \pm SD)

	Control Group (Group I) (N=10)	HFD Group (Group II) (N=10)	HFD + G-CSF Group (Group III) (N=10)	Significance test
Mean \pm SD	2.14 \pm 0.11	12.27 \pm 0.64	4.97 \pm 0.23	
P1		0.001<*	0.001<*	One-way ANOVA
P2			0.001<*	<i>P value</i> 0.001<*

Note: N: number, SD: standard deviation, P: Probability of ANOVA.

* : statistically significant ($P \leq 0.05$).

P1: Significance in relation to group I (control group). P2: Significance in relation to group II (HFD group).

Table 3: Area percentage of positive caspase-3 immune expression /HPF (X400) within study groups (Mean \pm SD)

	Control Group (Group I) (N=10)	HFD Group (Group II) (N=10)	HFD + G-CSF Group (Group III) (N=10)	Significance test
Mean \pm SD	0.45 \pm 0.14	15.93 \pm 0.17	4.75 \pm 0.19	
P1		0.001<*	0.001<*	One-way ANOVA
P2			0.001<*	<i>P value</i> 0.001<*

Note: N: number, SD: standard deviation, P: Probability of ANOVA.

* : statistically significant ($P \leq 0.05$).

P1: Significance in relation to group I (control group). P2: Significance in relation to group II (HFD group).

Table 4: Area percentage of positive CD117 immune expression in left ventricular sections /HPF (X400) within study groups (Mean \pm SD)

	Control Group (Group I) (N=10)	HFD Group (Group II) (N=10)	HFD + G-CSF Group (Group III) (N=10)	Significance test
Mean \pm SD	0.38 \pm 0.06	0.45 \pm 0.11	1.44 \pm 0.31	
P1		0.805	0.001<*	One-way ANOVA
P2			0.001<*	<i>P value</i> 0.001<*

Note: N: number, SD: standard deviation, P: Probability of ANOVA.

* : statistically significant ($P \leq 0.05$).

P1: Significance in relation to group I (control group). P2: Significance in relation to group II (HFD group).

Table 5: Area percentage of positive CD117 immune expression in right atrial sections /HPF (X400) within study groups (Mean \pm SD)

	Control Group (Group I) (N=10)	HFD Group (Group II) (N=10)	HFD + G-CSF Group (Group III) (N=10)	Significance test
Mean \pm SD	0.94 \pm 0.12	1.22 \pm 0.47	3.05 \pm 0.22	
P1		0.295	0.001<*	One-way ANOVA
P2			0.001<*	<i>P value</i> 0.001<*

Note: N: number, SD: standard deviation, P: Probability of ANOVA.

* : statistically significant ($P \leq 0.05$).

P1: Significance in relation to group I (control group). P2: Significance in relation to group II (HFD group).

Table 6: Number of caspase-3 immuno-positive cells /HPF (X400) within study groups (Mean ± SD)

	Control Group (Group I) (N=10)	HFD Group (Group II) (N=10)	HFD + G-CSF Group (Group III) (N=10)	Significance test
Mean ± SD	0.83 ± 0.75	24.17 ± 1.17	5.17 ± 1.47	
P1		0.001<*	0.001<*	One-way ANOVA P value 0.001<*
P2			0.001<*	

Note: N: number, SD: standard deviation, P: Probability of ANOVA.

* : statistically significant ($P \leq 0.05$).

P1: Significance in relation to group I (control group).

P2: Significance in relation to group II (HFD group).

Table 7: Number of CD117 immuno-positive cells in left ventricular sections /HPF (X400) within study groups (Mean ± SD)

	Control Group (Group I) (N=10)	HFD Group (Group II) (N=10)	HFD + G-CSF Group (Group III) (N=10)	Significance test
Mean ± SD	2.83 ± 0.75	3.67 ± 0.52	7.5 ± 1.05	
P1		0.204	0.001<*	One-way ANOVA P value 0.001<*
P2			0.001<*	

Note: N: number, SD: standard deviation, P: Probability of ANOVA.

* : statistically significant ($P \leq 0.05$).

P1: Significance in relation to group I (control group).

P2: Significance in relation to group II (HFD group).

Table 8: Number of CD117 immuno-positive cells in right atrial sections /HPF (X400) within study groups (Mean ± SD)

	Control Group (Group I) (N=10)	HFD Group (Group II) (N=10)	HFD + G-CSF Group (Group III) (N=10)	Significance test
Mean ± SD	5.5 ± 0.55	6.17 ± 0.75	14.83 ± 0.75	
P1		0.248	0.001<*	One-way ANOVA P value 0.001<*
P2			0.001<*	

Note: N: number, SD: standard deviation, P: Probability of ANOVA.

* : statistically significant ($P \leq 0.05$).

P1: Significance in relation to group I (control group).

P2: Significance in relation to group II (HFD group).

DISCUSSION

Worldwide, the intake of high-fat diets has been significantly increased due to major alterations in people's lifestyles. With little exercise, obesity and weight gain can result from a high-fat diet (HFD).^[22] Numerous changes in both structure and function of the myocardium linked to HFD can result in various types of cardiac impairment and failure.^[23] Granulocyte-colony stimulating factor (G-CSF) is a glycoprotein hematopoietic growth factor which can induce the precursor cells of neutrophils in the bone marrow to survive, proliferate, and differentiate.^[24,25] The aim of this research was to evaluate the role of G-CSF in amelioration of the changes that may occur in the cardiac muscle of adult male albino rats due to HFD intake and to assess the role of G-CSF in promoting cardiac muscle fiber repair mechanisms.

H&E-stained left ventricular sections of group II (HFD group) revealed significant degenerative alterations in the myocardium. Previous research has suggested that ROS (reactive oxygen species) overproduction contributes significantly to HFD-induced myocardial damage.^[26,27] This explains the significant increase in the level of malondialdehyde (MDA) in cardiac tissue homogenates of HFD group which is regarded as an oxidative stress biomarker. The majority of the cardiac muscle fibers in this group revealed hyper eosinophilic sarcoplasm in

H&E-stained sections. These findings coincide with the postulation of Dawood and Hareedy^[28] who reported that HFD-induced oxidative stress leads to compensatory rise in mitochondrial number and size (mitochondrial biogenesis) trying to maintain the normal function of the cardiac myocytes under stress. This finding was confirmed by ultrastructural examination of the cardiac myocytes of HFD group in the current study which revealed aggregations of numerous swollen mitochondria in the cardiac myocytes.

This oxidative stress induced by HFD caused significant changes in ultrastructure of various constituents of cardiac myocytes, including myofibrils, mitochondria, and plasma membrane. These ultrastructural alterations run in parallel with the light microscopic findings of current research. As regards the cardiac myofibrils, examination of the cardiac myocytes of HFD group revealed significant degenerative changes in ultrastructure of cardiac myofibrils in the form of disorganization and disruption. These changes could be attributed to oxidative injury to the cardiac myocytes by ROS.^[29] Bonda *et al*^[30] thought that the myofibrillar damage seen in their research was a result of mitochondrial dysfunction. Concerning the cardiac mitochondria, HFD group revealed significant mitochondrial morphological alterations in the form of deformation, variability in size and shape, and marked disorganization. Marques Neto *et al*^[31] documented that HFD-induced oxidative stress leads to subsequent opening of mPTP (mitochondrial

permeability transition pore) and suppression of the synthesis of ATP resulting in swelling and dysfunction of mitochondria. Regarding the cardiac myocyte's plasma membrane, corrugation and scalloping of the sarcolemma and subsarcolemmal accumulation of swollen mitochondria were demonstrated in group II. These results coincide with that of Dawood and Hareedy^[28] and Nabil *et al*^[32]. Omar *et al*^[33] demonstrated that ROS are extremely cytotoxic and induce membrane phospholipid peroxidation producing a noticeable deterioration and scalloping of the sarcolemma of cardiac myocytes.

On the contrary, H&E-stained left ventricular sections of group III (HFD + G-CSF group) demonstrated an apparent improvement in the structural alterations of the myocardium in comparison to group II (HFD group). Many previous studies have reported the antioxidant effect of G-CSF. Hou *et al*^[34] reported the protective role of G-CSF against the cardiac, hepatic, and renal damage caused by Adriamycin via the antioxidant effect of G-CSF. In the current research, this histological improvement could be correlated to the reduced level of MDA observed in this group which indicated diminution of oxidative stress.

This antioxidant effect of G-CSF caused noticeable improvement in ultrastructure of cardiac myofibrils, mitochondria, and plasma membrane. This ultrastructural improvement is consistent with the light microscopic observations of the current research. Regarding the cardiac myofibrils, there was marked improvement in myofibrillar ultrastructure in group III which may be mediated by G-CSF-induced upregulation of cardiac expression of GATA-4 which is an essential transcriptional factor that controls the expression of sarcomeric proteins like alpha-myosin heavy chain (MHC).^[35] In addition, G-CSF can protect the mitochondria of the cardiomyocytes during initial stages of heart damage through various mechanisms. Hiraumi *et al*^[36] reported that G-CSF can preserve cardiac mitochondria by enhancing ATP synthesis, and reestablishing the electron transport and oxygen utilization within the mitochondria primarily via complex IV. Furthermore, G-CSF has antioxidant impact on the myocardial cell membrane.^[33,37]

In group II, H&E-stained sections revealed variable-sized vacuolations in the majority of cardiac muscle fibers' sarcoplasm. This finding coincides with the work of Chiu *et al*^[38], Feriani *et al*^[39], and Ushakumari *et al*^[40] who declared that vacuolations may be an indication of intracellular lipid accumulation in cardiac myocytes. This finding was confirmed by ultrastructural examination of the cardiac myocytes of this group which revealed marked aggregations of variable-sized lipid droplets between the myofibrils and in the perinuclear areas. On the other hand, few muscle fibers of group III showed fewer vacuolations in their sarcoplasm. This finding was confirmed by ultrastructural examination of the cardiac myocytes of this group. Joo *et al*^[41] attributed this finding to G-CSF-induced enhancement of autophagy and thus decreasing lipid droplet accumulation in the cardiac myocytes.

By TEM, the intercalated discs (ICDs) of group II displayed irregularity and widening. Similar results were attained by Sibouakaz *et al*^[42] and Rasheed *et al*^[43]. Meng *et al*^[44] reported that connexin-40 (Cx40) and Cx43 expression, which are the primary connexins found at gap junctions of ICDs, is significantly downregulated by HFD, and their distribution is changed. On the other hand, ICDs in group III appeared normal with zigzag-like appearance. G-CSF can preserve ICDs by enhancing expression of Cx43 and controlling its phosphorylation and distribution through the JAK2-STAT3 pathway.^[45-47] Moreover, secondary lysosomes were detected in the sarcoplasm of cardiac myocytes of group II. Previous workers reported that HFD-induced impairment of autophagy is one of the primary causes of lysosome accumulation in cells.^[48]

In group II, marked deposition of blue-stained collagenous fibers in the endomysium among the cardiac muscle fibers and in the perivascular areas was demonstrated in Masson's trichrome-stained sections. These results run in parallel with that published by Shatoor and Al Humayed^[49]. This was confirmed by ultrastructural analysis of the myocardium of this group which revealed marked deposition of collagen fibrils in the endomysium. This result is consistent with a study published by Rasheed *et al*^[43]. Deposition of collagen observed in this group was also confirmed by the statistical results which indicated that the mean area percentage of the collagenous fibers in group II was significantly increased in comparison to the control group. Multiple mechanisms have been suggested to explain HFD-induced cardiac fibrosis. Sahraoui *et al*^[50] and Rasheed *et al*^[43] mentioned that fibrosis may be due to enhanced expression of pro- $\alpha 1$ chains of types I and III of collagen in the cardiac tissue. In addition, ER stress caused by HFD is a pro-fibrotic stimulus.^[51] On the contrary, Masson's trichrome-stained sections of group III demonstrated that perivascular and interstitial fibrosis was significantly reduced, as compared with group II. This was confirmed by ultrastructural myocardial examination of group III which demonstrated mild interstitial collagen deposition. This finding was also confirmed by the statistical results which exhibited a significant decrease in the mean area percentage of the collagenous fibers in group III in comparison to group II. These findings support the antifibrotic impact of G-CSF that has been previously documented.^[52] Szardien *et al*^[53] suggested that G-CSF reduces the fibrosis in the cardiac tissue by regulation of collagen production and breakdown in the extracellular matrix (ECM). They reported that G-CSF enhances matrix metalloproteinase-2 (MMP-2) and MMP-9 expressions leading to breakdown of excess collagen.

An obvious caspase-3 positive immune expression was observed in the cytoplasm and nuclei of the cardiac myocytes of group II. This observation was approved by the statistical findings that showed significant increases in the area percentage and the mean number of immunopositive cells for caspase-3 in group II in comparison to the control group. The increased caspase-3 expression as a

marker for apoptosis^[54] coincides with H&E results which revealed apoptotic nuclear changes in HFD group. There are several proposed mechanisms for the cardiomyocyte apoptosis caused by HFD, but oxidative stress is still the main reason^[55]. ROS overproduction causes cytochrome C to be released from mitochondria to the cytoplasm resulting in apoptosis.^[56] On the contrary, group III showed positive immune reaction of caspase-3 in the cytoplasm of few cardiac myocytes, in comparison to group II. This was represented statistically by a significant reduction in the area percentage and the mean number of immuno-positive cells for caspase-3. Buddhala *et al*^[57] reported that G-CSF prevents apoptosis by preserving mPTP via inhibition of mPTP opening.

In the present study, CD117 (C-kit) antibody is used as a marker for cardiac stem cells (CSCs).^[58] CSCs are a diverse group of cells which live in distinct stem cell niches in particular regions of the normal human heart^[15,59] McQuaig *et al*^[60] and Sjölin *et al*^[61] demonstrated that the highest concentrations of CSCs are thought to be found in the right atrium, right atrial appendage, right atrioventricular junction, and base of the tricuspid valve. Telocytes (TCs) are type of interstitial cells that reside in the stem cell niches of several organs, including the heart, participate in tissue regeneration, and also express CD117^[62,63].

Immunohistochemical stained sections of the right atrium of the control group for C-kit immune reaction showed positive immune reaction represented in resident (endogenous) cardiac stem cells and telocytes in the C.T. endomysium among the cardiac muscle fibers. However, the sections of the left ventricle revealed positive immune reaction in relatively fewer cardiac stem cells and telocytes among the cardiac muscle fibers. These results are in accordance with those of Arsalan *et al*^[64] and Li, Guo, *et al*^[65] who showed that the atria have a higher concentration of CSCs compared to the ventricles. Furthermore, minimal injury may occur in the normal hearts resulting in very low rates of apoptosis^[66,67] promoting stem cell migration from the atrium to the ventricle.

These C-kit positive cells are mostly cardiac stem cells. This is explained by the significant increase in C-kit immune expression in group III (HFD + G-CSF group) by G-CSF-mediated mobilization of hematopoietic stem cells. Furthermore, Ceausu *et al*^[15] reported that CSCs were recognized by their intimate adherence to cardiac myocytes. They were found in the peri-fibrillar and interstitial spaces, in close proximity to the sarcolemma of the cardiac muscle fibers. From a morphological perspective, CSCs are small, plump, ovoid cells with clearly defined borders. This is supported by ultrastructural examination of the myocardium in all groups which revealed cardiac stem cells and telocytes in the endomysium. In addition, CSCs have been isolated from a variety of animal models using selection based on CD117 expression.^[68] The progenitor marker CD117 has been used to differentiate between endothelial cells and endothelial progenitor cells (EPCs) (type of CSCs). Endothelial cells can express multiple

endothelial markers, including CD31, CD34, CD144, CD146, and KDR, while EPCs are positive for CD117.^[69]

On the other hand, HFD group revealed non-significant increases in the area percentage and the mean number of C-kit immuno-positive cells. Importantly, the cardiac injury in any heart disease causes an increase in C-kit expression^[70] as an attempt to initiate the repair process. Li *et al*^[65] reported an increase in cardiac expression of C-kit in heart failure through stem cell mobilization to the sites of tissue damage that need repair. Regarding group III, immune expression of C-kit in both left ventricular and right atrial sections was significantly increased, in comparison to group II. This was supported statistically by a significant increase in the area percentage and the mean number of immuno-positive cells for C-Kit. This indicates that G-CSF effectively promotes bone marrow-derived hematopoietic stem cell (HSC) mobilization and enhances their homing to the sites of cardiac injury. Such findings coincide with that published by Huber *et al*^[71], Gross *et al*^[72], and Ghanimati *et al*^[24]. In addition to the capability of the positive cells for C-kit to differentiate into cardiomyogenic or vasculogenic lineage after myocardial injury, they can trigger additional processes like neo-angiogenesis, apoptosis suppression, ECM remodeling, and activation of additional stem cells resulting in cardiac regeneration.^[24,58,73]

Ultrastructural examination of the endomysium of the right atrium of the control group showed resident CSCs having euchromatic centrally located nuclei and little cytoplasm with high nuclear to cytoplasmic ratio. Telocytes with euchromatic nuclei and cytoplasmic processes (telopodes) were also observed. These results coincide with those published by Gherghiceanu *et al*^[74], Ceausu *et al*^[15], Gawad *et al*^[75], and Shati *et al*^[76]. Regarding group II, the stem cells had euchromatic nuclei. However, the telocytes had condensed irregular nuclei and marked cytoplasmic vacuolations. In cardiomyopathy, oxidative stress has a deleterious effect on telocyte formation by apoptosis. Previous studies reported that telocytes can endure this hostility, but only with changes to their ultrastructure that include cytoplasmic vacuolations.^[63,77,78] The stem cells in group III had euchromatic nuclei. Some telocytes appeared normal, others exhibited cytoplasmic vacuolations. Omar *et al*^[79] demonstrated that telocytes are preserved by G-CSF through G-CSF's protective impact on telocytes as well as the ability of G-CSF to mobilize hematopoietic stem cells. Therefore, the preserved telocytes can serve the cardiac myocytes by providing support to the cardiac myocytes and by the nursing effect for stem cells.^[79,80]

CONCLUSION

From this study, it is possible to reach the conclusion that HFD negatively impacts the microscopic structure of the cardiac muscle of adult rats. Therefore, diet control and avoidance of HFD are recommended to protect the cardiovascular system from such effects. G-CSF has a promising role in amelioration of HFD harmful effects on

the myocardium. Further clinical studies and investigations such as ECG, Echo and biochemical analysis for cardiac enzymes are needed for accurate evaluation of the cardioprotective role of G-CSF against HFD-induced cardiotoxicity as well as assessment of the safety of G-CSF use.

CONFLICT OF INTERESTS

There are no conflicts of interest.

REFERENCES

1. Dutta M, Ghosh D, Ghosh AK, Bose G, Chattopadhyay A, Rudra S, Dey M, Bandyopadhyay A, Pattari SK, Mallick S. High fat diet aggravates arsenic induced oxidative stress in rat heart and liver. *Food Chem Toxicol.* 2014;66:262-277. <https://doi.org/10.1016/j.fct.2014.01.050>
2. Charradi K, Sebai H, Elkahoui S, Hassine FB, Limam F, Aouani E. Grape seed extract alleviates high-fat diet-induced obesity and heart dysfunction by preventing cardiac siderosis. *Cardiovasc Toxicol.* 2011;11(1): 28-37. <https://doi.org/10.1007/s12012-010-9101-z>
3. Zhang Y, Yuan M, Bradley KM, Dong F, Anversa P, Ren J. IGF-1 alleviates high fat diet-induced myocardial contractile dysfunction: role of insulin signaling and mitochondrial function. *Hypertension.* 2012;59(3):680. <https://doi.org/10.1161/HYPERTENSIONAHA.111.181867>
4. Jang H, Conklin DJ, Kong M. Piecewise nonlinear mixed-effects models for modeling cardiac function and assessing treatment effects. *Comput Methods Programs Biomed.* 2013;110(3):240-252. <https://doi.org/10.1016/j.cmpb.2012.11.007>
5. Sun W, Zhang Z, Chen Q, Yin X, Fu Y, Zheng Y, Cai L, Kim K-S, Kim KH, Tan Y. Magnolia extract (BL153) protection of heart from lipid accumulation caused cardiac oxidative damage, inflammation, and cell death in high-fat diet fed mice. *Oxid Med Cell Longev.* 2014;2014:1-14. <https://doi.org/10.1155/2014/205849>
6. Harada M, Qin Y, Takano H, Minamino T, Zou Y, Toko H, Ohtsuka M, Matsuura K, Sano M, Nishi J-i. G-CSF prevents cardiac remodeling after myocardial infarction by activating the Jak-Stat pathway in cardiomyocytes. *Nat Med.* 2005;11(3):305-311. <https://doi.org/10.1038/nm1199>
7. Xiao BG, Lu CZ, Link H. Cell biology and clinical promise of G-CSF: immunomodulation and neuroprotection. *J Cell Mol Med.* 2007;11(6): 1272-1290. <https://doi.org/10.1111/j.1582-4934.2007.00101.x>
8. Forechi L, Baldo MP, Meyerfreund D, Mill JG. Granulocyte colony-stimulating factor improves early remodeling in isoproterenol-induced cardiac injury in rats. *Pharmacol Rep.* 2012;64(3):643-649. [https://doi.org/10.1016/S1734-1140\(12\)70860-5](https://doi.org/10.1016/S1734-1140(12)70860-5)
9. Park I-H, Song Y-S, Joo H-W, Shen G-Y, Seong J-H, Shin N-K, Cho YJ, Lee Y, Shin JH, Lim Y-H. Role of microRNA-34a in anti-apoptotic effects of granulocyte-colony stimulating factor in diabetic cardiomyopathy. *Diabetes Metab J.* 2020;44(1): 173-185. <https://doi.org/10.4093/dmj.2018.0211>
10. Andrade D, Oliveira G, Menezes L, Nascimento AL, Carvalho S, Stumbo AC, Thole A, Garcia-Souza É, Moura A, Carvalho L. Insulin-like growth factor-1 short-period therapy improves cardiomyopathy stimulating cardiac progenitor cells survival in obese mice. *Nutr Metab Cardiovasc Dis.* 2020;30(1):151-161. <https://doi.org/10.1016/j.numecd.2019.09.001>
11. Farhangi MA, Nameni G, Hajiluan G, Mesgari-Abbasi M. Cardiac tissue oxidative stress and inflammation after vitamin D administrations in high fat-diet induced obese rats. *BMC Cardiovasc Disord.* 2017;17(1):161. <https://doi.org/10.1186/s12872-017-0597-z>
12. Suvarna SK, Layton C, Bancroft JD. Bancroft's Theory and Practice of Histological Techniques. 8th ed. Elsevier; 2018:126-166.
13. Jackson P, Blythe D. Immunohistochemical techniques. In: Suvarna KS, Layton C, Bancroft JD, eds. Bancroft's Theory and Practice of Histological Techniques: Expert Consult: Online and Print. 7th ed. Elsevier Health Sciences; 2012:381-427:chap 18.
14. Lokman MS, Althagafi HA, Alharthi F, Habotta OA, Hassan AA, Elhefny MA, Al Sberi H, Theyab A, Mufti AH, Alhazmi A. Protective effect of quercetin against 5-fluorouracil-induced cardiac impairments through activating Nrf2 and inhibiting NF-κB and caspase-3 activities. *Environ Sci Pollut Res.* 2023;30(7): 17657-17669. <https://doi.org/10.1007/s11356-022-23314-z>
15. Ceausu Z, Socea B, Dimitriu MC, Predescu D, Constantin VD, Bacalbaşa N, Cirstoveanu C, Costache M, Ceausu M. Dormant cardiac stem cells: A promising tool in cardiac regeneration. *Exp Ther Med.* 2020;20(4):3452-3457. <https://doi.org/10.3892/etm.2020.9015>
16. Nakamura Y, Maekawa T, Felizola SJ, Satoh F, Qi X, Velarde-Miranda C, Plonczynski MW, Ise K, Kikuchi K, Rainey WE. Adrenal CYP11B1/2 expression in primary aldosteronism: immunohistochemical analysis using novel monoclonal antibodies. *Mol Cell Biochem.* 2014;392(1-2):73-79. <https://doi.org/10.1016/j.mce.2014.05.002>
17. Bhosale PG, Kennedy RA, Watt FM. Caspase activation in tumour-infiltrating lymphocytes is associated with lymph node metastasis in oral squamous cell carcinoma. *J Pathol.* 2023;261(1): 43-54. <https://doi.org/10.1002/path.6145>

18. Lin S-C, Yen H-H, Lee P-C, Lai I-R. Oncological outcomes of large gastrointestinal stromal tumors treated by laparoscopic resection. *Surg Endosc.* 2023;37(3):2021-2028. <https://doi.org/10.1007/s00464-022-09693-x>
19. Woods AE, Stirling JW. Transmission electron microscopy. In: Suvarna SK, Layton C, Bancroft JD, eds. *Bancroft's Theory and Practice of Histological Techniques*. 8th ed. Elsevier Health Sciences; 2018:434-476.
20. Noeman SA, Hamooda HE, Baalash AA. Biochemical study of oxidative stress markers in the liver, kidney and heart of high fat diet induced obesity in rats. *Diabetol Metab Syndr.* 2011;3(1):1-8. <https://doi.org/10.1186/1758-5996-3-17>
21. Rosner B. *Fundamentals of Biostatistics*. 8th ed. Cengage Learning; 2015:516-587.
22. Elrashidy RA. Dysregulation of nuclear factor erythroid 2-related factor 2 signaling and activation of fibrogenic pathways in hearts of high fat diet-fed rats. *Mol Biol Rep.* 2020;47(4):2821-2834. <https://doi.org/10.1007/s11033-020-05360-3>
23. Abu-Elsaad N, El-Karef A. The falconoid luteolin mitigates the myocardial inflammatory response induced by high-carbohydrate/high-fat diet in wistar rats. *Inflammation.* 2018;41:221- 231. <https://doi.org/10.1007/s10753-017-0680-8>
24. Ghanimati R, Rajabi H, Ramezani F, Ramez M, Bapiran M, Nasirinezhad F. The effect of preconditioning with high-intensity training on tissue levels of G-CSF, its receptor and C-kit after an acute myocardial infarction in male rats. *BMC Cardiovasc Disord.* 2020;20(1):1-9. <https://doi.org/10.1186/s12872-020-01380-w>
25. Chen Z, Ren X, Ren R, Wang Y, Shang J. The combination of G-CSF and AMD3100 mobilizes bone marrow-derived stem cells to protect against cisplatin-induced acute kidney injury in mice. *Stem Cell Res Ther.* 2021;12:1-13. <https://doi.org/10.1186/s13287-021-02268-y>
26. Reaven G, Abbasi F, McLaughlin T. Obesity, insulin resistance, and cardiovascular disease. *Recent Prog Horm Res.* 2004;59:207-224.
27. Ritchie RH, Drummond GR, Sobey CG, De Silva TM, Kemp-Harper BK. The opposing roles of NO and oxidative stress in cardiovascular disease. *Pharmacol Res.* 2017;116:57-69. <https://doi.org/10.1016/j.phrs.2016.12.017>
28. Dawood A, Hareedy H. Differential effect of high fat diet (HFD) on the cardiac muscle of adult and aged female mice and the possible protective role of artichoke treatment: histomorphometric and ultrastructural study. *J Med Histol.* 2019;3(1):36-54. DOI: 10.21608/jmh.2019.11528.1053
29. Elmas MA, Cakıcı SE, Dur IR, Kozluca I, Arınc M, Binbuga B, Ozakpınar OB, Kolgazi M, Sener G, Ercan F. Protective effects of exercise on heart and aorta in high-fat diet-induced obese rats. *Tissue and Cell.* 2019;57:57-65. <https://doi.org/10.1016/j.tice.2019.01.005>
30. Bonda TA, Szynaka B, Sokołowska M, Dziemidowicz M, Waszkiewicz E, Winnicka MM, Bernaczyk P, Wawrusiewicz-Kurylonek N, Kamiński KA. Interleukin 6 modulates PPAR α and PGC-1 α and is involved in high-fat diet induced cardiac lipotoxicity in mouse. *Int J Cardiol.* 2016;219:1-8. <https://doi.org/10.1016/j.ijcard.2016.05.021>
31. Marques Neto SR, Castiglione RC, da Silva TC, Paes LdS, Pontes A, Oliveira DF, Ferraz EB, Ade Caldas CC, Nascimento JHM, Bouskela E. Effects of high intensity interval training on neuro-cardiovascular dynamic changes and mitochondrial dysfunction induced by high-fat diet in rats. *PLoS One.* 2020;15(10):e0240060. <https://doi.org/10.1371/journal.pone.0240060>
32. Nabil IM, Ahmed WAR, El Sabeh SS, Abouelrous RA, ElSekily NM. The possible protective effect of aldehyde dehydrogenase 2 agonist (alda-1) on doxorubicin induced toxicity of the left ventricular cardiomyocytes of adult male mice. *Egypt J Histol.* 2022;45(1):50-67. DOI: 10.21608/EJH.2021.58210.1418
33. Omar AM, Meleis AE, Arfa SA, Zahran NM, Mehanna RA. Comparative study of the therapeutic potential of mesenchymal stem cells derived from adipose tissue and bone marrow on acute myocardial infarction model. *Oman Med J.* 2019;34(6):534. doi: 10.5001/omj.2019.97
34. Hou X-W, Jiang Y, Wang L-F, Xu H-Y, Lin H-M, He X-Y, He J-J, Zhang S. Protective role of granulocyte colony-stimulating factor against adriamycin induced cardiac, renal and hepatic toxicities. *Toxicol Lett.* 2009;187(1):40-44. <https://doi.org/10.1016/j.toxlet.2009.01.025>
35. Pourtaji A, Jahani V, Moallem SM, Mohammadpour AH. Application of G-CSF in congestive heart failure treatment. *Curr Cardiol Rev.* 2019;15(2):83-90. <https://doi.org/10.2174/1573403X14666181031115118>
36. Hiraumi Y, Iwai-Kanai E, Baba S, Yui Y, Kamitsuji Y, Mizushima Y, Matsubara H, Watanabe M, Watanabe K-i, Toyokuni S. Granulocyte colony-stimulating factor protects cardiac mitochondria in the early phase of cardiac injury. *Am J Physiol-Heart Circ Physiol.* 2009;296(3):H823-H832. <https://doi.org/10.1152/ajpheart.00774.2008>
37. Villalón-García I, Povea-Cabello S, Álvarez-Córdoba M, Talaverón-Rey M, Suárez-Rivero JM, Suárez-Carrillo A, Munuera-Cabeza M, Reche-López D, Cilleros-Holgado P, Piñero-Pérez R. Vicious cycle of lipid peroxidation and iron accumulation in neurodegeneration. *Neural Regen Res.* 2023;18(6):1196. doi: 10.4103/1673-5374.358614

38. Chiu H-C, Kovacs A, Ford DA, Hsu F-F, Garcia R, Herrero P, Saffitz JE, Schaffer JE. A novel mouse model of lipotoxic cardiomyopathy. *J Clin Invest.* 2001;107(7):813-822. <https://doi.org/10.1172/JCI10947>
 39. Feriani A, Bizzarri M, Tir M, Aldawood N, Alobaid H, Allagui MS, Dahmash W, Tlili N, Mnafigui K, Alwasel S. High-fat diet-induced aggravation of cardiovascular impairment in permethrin-treated Wistar rats. *Ecotoxicol Environ Saf.* 2021;222:112461. <https://doi.org/10.1016/j.ecoenv.2021.112461>
 40. Ushakumari CJ, Zhou QL, Wang Y-H, Na S, Rigor MC, Zhou CY, Kroll MK, Lin BD, Jiang ZY. Neutrophil elastase increases vascular permeability and leukocyte transmigration in cultured endothelial Cells and obese mice. *Cells.* 2022;11(15):2288. <https://doi.org/10.3390/cells11152288>
 41. Joo H-W, Song Y-S, Park I-H, Shen G-Y, Seong J-H, Shin N-K, Lee A, Kim H, Kim K-S. Granulocyte colony stimulating factor ameliorates hepatic steatosis associated with improvement of autophagy in diabetic rats. *Can J Gastroenterol Hepatol.* 2020;2020:1-9. <https://doi.org/10.1155/2020/2156829>
 42. Sibouakaz D, Othmani-Mecif K, Fernane A, Taghliat A, Benazzoug Y. Biochemical and ultrastructural cardiac changes induced by high-fat diet in female and male prepubertal rabbits. *Anal Cell Pathol.* 2018;2018:1-17. <https://doi.org/10.1155/2018/6430696>
 43. Rasheed R, Othman M, Hussein U. The possible ameliorative influence of quercetin on cardiac muscle changes induced by high fat diet in adult male albino rats: light and electron microscopic study. *Egypt J Histol.* 2022;45(3):937-948. DOI: 10.21608/ejh.2021.76868.1484
 44. Meng T, Cheng G, Wei Y, Ma S, Jiang Y, Wu J, Zhou X, Sun C. Exposure to a chronic high-fat diet promotes atrial structure and gap junction remodeling in rats. *Int J Mol Med.* 2017;40(1):217-225. <https://doi.org/10.3892/ijmm.2017.2982>
 45. Liu H-M, Luo T, Zhou X, Cai L, Huang T-G, Jiang T-M, Li Y-M. Disassociation between left ventricular mechanical and electrical properties in ischemic rat heart after G-CSF treatment. *Cardiovasc Drugs Ther.* 2011;25(3):203-214. <https://doi.org/10.1007/s10557-011-6294-8>
 46. Solan JL, Lampe PD. Spatio-temporal regulation of connexin43 phosphorylation and gap junction dynamics. *Biochim Biophys Acta -Biomembranes.* 2018;1860(1):83-90. <https://doi.org/10.1016/j.bbmem.2017.04.008>
 47. Wang W, Ye S, Zhang L, Jiang Q, Chen J, Chen X, Zhang F, Wu H. Granulocyte colony-stimulating factor attenuates myocardial remodeling and ventricular arrhythmia susceptibility via the JAK2-STAT3 pathway in a rabbit model of coronary microembolization. *BMC Cardiovasc Disord.* 2020;20(1):1-12. <https://doi.org/10.1186/s12872-020-01385-5>
 48. Mizunoe Y, Sudo Y, Okita N, Hiraoka H, Mikami K, Narahara T, Negishi A, Yoshida M, Higashibata R, Watanabe S. Involvement of lysosomal dysfunction in autophagosome accumulation and early pathologies in adipose tissue of obese mice. *Autophagy.* 2017;13(4):642-653. <https://doi.org/10.1080/15548627.2016.1274850>
 49. Shatoor AS, Al Humayed S. Astaxanthin Ameliorates high-fat diet-induced cardiac damage and fibrosis by upregulating and activating SIRT1. *Saudi J Biol Sci.* 2021;28(12):7012-7021. <https://doi.org/10.1016/j.sjbs.2021.07.079>
 50. Sahraoui A, Dewachter C, De Medina G, Naeije R, Aouichat Bouguerra S, Dewachter L. Myocardial structural and biological anomalies induced by high fat diet in *Psammomys obesus* gerbils. *PLoS One.* 2016;11(2):e0148117. <https://doi.org/10.1371/journal.pone.0148117>
 51. Yang J, Liang C, Liu L, Wang L, Yu G. High-Fat Diet Related Lung Fibrosis-Epigenetic Regulation Matters. *Biomolecules.* 2023;13(3):558. <https://doi.org/10.3390/biom13030558>
 52. Aktaş A, Aşır F, Başaran SÖ, Kaplan Ö, Ermiş IS, Deveci E. Granulocyte colony stimulating factor (GCSF) protected in ovarian tissues against ischemia-reperfusion injury. *J drug deliv ther.* 2022;12(4):26-30. <https://doi.org/10.22270/jddt.v12i4.5538>
 53. Szardien S, Nef HM, Voss S, Troidl C, Liebetrau C, Hoffmann J, Rauch M, Mayer K, Kimmich K, Rolf A. Regression of cardiac hypertrophy by granulocyte colony-stimulating factor-stimulated interleukin-1 β synthesis. *Eur Heart J.* 2012;33(5):595-605. <https://doi.org/10.1093/eurheartj/ehr434>
 54. Lu Q, Zheng R, Zhu P, Bian J, Liu Z, Du J. Hinokinin alleviates high fat diet/streptozotocin-induced cardiac injury in mice through modulation in oxidative stress, inflammation and apoptosis. *Biomed Pharmacother.* 2021;137:111361. <https://doi.org/10.1016/j.biopha.2021.111361>
 55. Meng M, Jia R, Wei M, Meng X, Zhang X, Du R, Sun W, Wang L, Song L. Oxidative stress activates Ryr2-Ca²⁺ and apoptosis to promote PM2.5-induced heart injury of hyperlipidemia mice. *Ecotoxicol Environ Saf.* 2022;232:113228. <https://doi.org/10.1016/j.ecoenv.2022.113228>
 56. Jiménez-González S, Marín-Royo G, Jurado-López R, Bartolomé MV, Romero-Miranda A, Luaces M, Islas F, Nieto ML, Martínez-Martínez E, Cachofeiro V. The crosstalk between cardiac lipotoxicity and mitochondrial oxidative stress in the cardiac alterations in diet-induced obesity in rats. *Cells.* 2020;9(2):451. <https://doi.org/10.3390/cells9020451>
-

57. Buddhala C, Prentice H, Wu J-Y. Modes of action of taurine and granulocyte colony-stimulating factor in neuroprotection. *J Exp Clin Med.* 2012;4(1):1-7. <https://doi.org/10.1016/j.jecm.2011.11.001>
58. Marino F, Scalise M, Cianflone E, Mancuso T, Aquila I, Agosti V, Torella M, Paolino D, Mollace V, Nadal-Ginard B. Role of c-kit in myocardial regeneration and aging. *Front Endocrinol.* 2019;10:371. <https://doi.org/10.3389/fendo.2019.00371>
59. Cianflone E, Torella M, Biamonte F, De Angelis A, Urbanek K, Costanzo FS, Rota M, Ellison-Hughes GM, Torella D. Targeting cardiac stem cell senescence to treat cardiac aging and disease. *Cells.* 2020;9(6):1558. <https://doi.org/10.3390/cells9061558>
60. McQuaig R, Dixit P, Yamauchi A, Van Hout I, Papannarao JB, Bunton R, Parry D, Davis P, Katare R. Combination of cardiac progenitor cells from the right atrium and left ventricle exhibits synergistic paracrine effects *in vitro*. *Cell Transplant.* 2020;29:1-13. <https://doi.org/10.1177/0963689720972328>
61. Sjölin J, Jonsson M, Orback C, Oldfors A, Jeppsson A, Synnergren J, Rotter Sopasakis V, Vukusic K. Expression of stem cell niche-related biomarkers at the base of the human tricuspid valve. *Stem Cells Dev.* 2023;32(5-6):140-151. <https://doi.org/10.1089/scd.2022.0253>
62. Radu BM, Banciu A, Banciu DD, Radu M, Cretoiu D, Cretoiu SM. Calcium signaling in interstitial cells: focus on telocytes. *Int J Mol Sci.* 2017;18(2):397. <https://doi.org/10.3390/ijms18020397>
63. Condrat CE, Barbu MG, Thompson DC, Dănilă CA, Boboc AE, Suci N, Crețoiu D, Voinea SC. Roles and distribution of telocytes in tissue organization in health and disease. In: Gorbunov NV, ed. *Tissue Barriers in Disease, Injury and Regeneration.* 1st ed. Elsevier; 2021:1-41:chap 1. <https://doi.org/10.1016/B978-0-12-818561-2.00001-1>
64. Arsalan M, Woitek F, Adams V, Linke A, Barten MJ, Dhein S, Walther T, Mohr F-W, Garbade J. Distribution of cardiac stem cells in the human heart. *Int Sch Res Notices.* 2012;2012:1-5. doi:10.5402/2012/483407
65. Li S, Guo K, Wu J, Guo Z, Li A. Altered expression of c-kit and nanog in a rat model of Adriamycin-induced chronic heart failure. *Am J Cardiovasc Dis.* 2017;7(2):57. PMID: 28533931; PMCID: PMC5435606.
66. González A, Fortuño MaA, Querejeta R, Ravassa S, López B, López N, Díez J. Cardiomyocyte apoptosis in hypertensive cardiomyopathy. *Cardiovasc Res.* 2003;59(3):549-562. [https://doi.org/10.1016/S0008-6363\(03\)00498-X](https://doi.org/10.1016/S0008-6363(03)00498-X)
67. Tsipis A. Heart muscle and apoptosis. In: Veselka J, ed. *Cardiomyopathies-From Basic Research to Clinical Management.* 1st ed. IntechOpen; 2012:185-198.
68. Ellison GM, Galuppo V, Vicinanza C, Aquila I, Waring CD, Leone A, Indolfi C, Torella D. Cardiac stem and progenitor cell identification: different markers for the same cell. *Front Biosci.* 2010;2:641-652.
69. Lachmann R, Lanuti P, Miscia S. OMIP-011: Characterization of circulating endothelial cells (CECs) in peripheral blood. *Cytometry A.* 2012;81(7):549-551. DOI: 10.1002/cyto.a.22071
70. Shinohara D, Matsushita S, Yamamoto T, Inaba H, Kuwaki K, Shimada A, Amano A. Reduction of c-kit positive cardiac stem cells in patients with atrial fibrillation. *J Cardiol.* 2017;69(5):712-718. <https://doi.org/10.1016/j.jjcc.2016.07.006>
71. Huber BC, Beetz NL, Laskowski A, Ziegler T, Grabmaier U, Kupatt C, Herbach N, Wanke R, Franz WM, Massberg S. Attenuation of cardiac hypertrophy by G-CSF is associated with enhanced migration of bone marrow-derived cells. *J Cell Mol Med.* 2015;19(5):1033-1041. <https://doi.org/10.1111/jcmm.12494>
72. Gross L, Paintmayer L, Lehner S, Brandl L, Brenner C, Grabmaier U, Huber B, Bartenstein P, Theiss H-D, Franz W-M. FDG-PET reveals improved cardiac regeneration and attenuated adverse remodelling following Sitagliptin+ G-CSF therapy after acute myocardial infarction. *Eur Heart J Cardiovasc Imaging.* 2016;17(2):136-145. <https://doi.org/10.1093/ehjci/jev237>
73. Li M, Wang Z, Xia H, Yu L, Hu Z. Vildagliptin and G-CSF improved angiogenesis and survival after acute myocardial infarction. *Arch Med Res.* 2019;50(3):133-141. <https://doi.org/10.1016/j.arcmed.2019.07.004>
74. Gherghiceanu M, Popescu L. Cardiomyocyte precursors and telocytes in epicardial stem cell niche: electron microscope images. *J Cell Mol Med.* 2010;14(4):871-877. <https://doi.org/10.1111/j.1582-4934.2010.01060.x>
75. Gawad SKA, Al-Shahed FA-ZN, Abd El-Zaher MH. Histological and immunohistochemical study of telocytes in the heart of male albino rats in different age groups. *Sci j Al-Azhar med fac girls.* 2020;4(3):373-382. DOI: 10.4103/sjamf.sjamf_43_20
76. Shati AA, Zaki MSA, Alqahtani YA, Haidara MA, Al-Shraim M, Dawood AF, Eid RA. Potential protective effect of vitamin C on Qunalphos-induced cardiac toxicity: histological and tissue biomarker assay. *Biomedicines.* 2021;10(1):39. <https://doi.org/10.3390/biomedicines10010039>
77. Enciu A-M, Popescu LM. Telopodes of telocytes are influenced *in vitro* by redox conditions and ageing. *Mol Cell Biochem.* 2015;410:165-174. <https://doi.org/10.1007/s11010-015-2548-2>
78. Kostin S. Cardiac telocytes in normal and diseased hearts. *Semin Cell Dev Biol.* 2016;55:22-30. <https://doi.org/10.1016/j.semdb.2016.02.023>

79. Omar AI, Yousry MM, Farag EA. Therapeutic mechanisms of granulocyte-colony stimulating factor in methotrexate-induced parotid lesion in adult rats and possible role of telocytes: a histological study. *Egypt J Histol.* 2018;41(1):93-107. DOI: 10.21608/EJH.2018.7525
80. Choobineh S, Borjian Fard M, Soori R, Mazaheri Z. Telocytes response to cardiac growth induced by resistance exercise training and endurance exercise training in adult male rats. *J Physiol Sci.* 2023;73(1):1-12. <https://doi.org/10.1186/s12576-023-00868-2>

الملخص العربي

التأثير المخفف المحتمل لعامل تحفيز مستعمرات خلايا الدم البيضاء المحببة على اعتلال عضلة القلب الناجم عن النظام الغذائي عالي الدهون في الجرذان البيضاء: دراسة نسيجية وهستوكيميائية مناعية ودراسة التركيب الدقيق

سارة مجدي عبد الهادي السعيد، شهاب حافظ محمد، نسرین مصطفى عمر، ایمان شعبان عبد العزيز أبو العلا
قسم علم الأنسجة الطبية وبيولوجيا الخلية- كلية الطب- جامعة المنصورة

الخلفية: عادة ما يرتبط تناول نظام غذائي عالي الدهون (HFD) لفترات طويلة بالسمنة وزيادة خطر الإصابة بأمراض متعددة بما في ذلك داء السكري من النوع الثاني، واضطرابات القلب والأوعية الدموية، وارتفاع ضغط الدم، وكذلك زيادة الدهون في الدم. عامل تحفيز مستعمرة الخلايا المحببة (G-CSF) هو سيتوكين متعدد الببتيد يشارك في التحكم الأساسي في إنتاج الخلايا المتعادلة.

الهدف من البحث: تم إجراء الدراسة الحالية لاستقصاء دور G-CSF في اعتلال عضلة القلب الناجم عن HFD في نموذج الفئران.

مواد وطرق البحث: تم استخدام ثلاثين من ذكور الجرذان البيضاء البالغة (٢٠٠-٢٢٠ جرام) وتم تقسيمهم إلى ثلاث مجموعات. المجموعة الأولى (المجموعة الضابطة): تم تغذيتها على نظام غذائي قياسي لمدة ١٤ أسبوعاً. المجموعة الثانية (مجموعة HFD): تم تغذيتها على HFD لمدة ١٤ أسبوعاً. المجموعة الثالثة (HFD + G-CSF) تم تغذيتها على HFD لمدة ١٤ أسبوعاً وتعطى G-CSF (٢٠٠ ميكروجرام / كجم / يوم) داخل التجويف البريتوني مرة واحدة يومياً لمدة ٥ أيام متتالية تبدأ بعد ١٢ أسبوعاً من تناول HFD. تم الحصول على عينات من البطين الأيسر والأذين الأيمن ومعالجتها للدراسات المجهرية الضوئية والإلكترونية. تم إجراء الدراسات البيوكيميائية والهستومورفومترية (النسيجية) والإحصائية.

النتائج: أظهرت مجموعة HFD تغيرات وتدهور ملحوظ في عضلة القلب على مستوى المجهر الضوئي والإلكتروني. رافقت هذه التغييرات زيادات كبيرة في مستوى MDA للأنسجة ونسبة مساحة الكولاجين والتفاعل المناعي الإيجابي ل-caspase ٣. من ناحية أخرى، أظهرت مجموعة HFD + G-CSF تحسناً في أنسجة عضلة القلب مع انخفاض في مستوى MDA في الأنسجة ونسبة مساحة الكولاجين والتفاعل المناعي الإيجابي ل-caspase ٣. ولوحظ أيضاً زيادة التفاعل المناعي الإيجابي ل CD١١٧ في هذه المجموعة.

الاستنتاج: يمكن لـ G-CSF أن يخفف بشكل كبير من السمية القلبية بسبب HFD من خلال التأثيرات المضادة للأكسدة والمضادة لموت الخلايا المبرمج والمضادة للتليف وتحريك الخلايا الجذعية المشتقة من نخاع العظمي إلى الأنسجة المصابة.